J. Man, P. Klapetek, O. Man, A. Weidner, K. Obrtlík and J. Polák: Extrusions and intrusions in fatigued metals. Part 2. AFM and EBSD study of the early growth of extrusions and intrusions in 316L steel fatigued at room temperature

Jiri Man, Petr Klapetek, Ondrej Man, Anja Weidner, Karel Obrtlik, Jaroslav Polak

J. Man, P. Klapetek, O. Man, A. Weidner, K. Obrtlík and J. Polák: Extrusions and intrusions in fatigued metals. Part 2. AFM and EBSD study of the early growth of extrusions and intrusions in 316L steel fatigued at room temperature

Journal:	*Philosophical Magazine & Philosophical Magazine Letters*
Manuscript ID:	TPHM-08-Nov-0448.R1
Journal Selection:	Philosophical Magazine
Date Submitted by the Author:	12-Mar-2009
Complete List of Authors:	Man, Jiri; Institute of Physics of Materials, ASCR Klapetek, Petr; Czech Metrology Institute Man, Ondrej; Brno University of Technology, Institute of Materials Science and Engineering Weidner, Anja; Technische Universität Bergakademie Freiberg, Institute of Material Science Obrtlik, Karel; Institute of Physics of Materials, ASCR Polak, Jaroslav; Institute of Physics of Materials, ASCR
Keywords:	AFM, cyclic deformation, EBSD, experimental, fatigue, FIB, slip bands, steel
Keywords (user supplied):	persistent slip marking, extrusion, intrusion

RESEARCH ARTICLE

Extrusions and intrusions in fatigued metals. Part 2. AFM and EBSD study of the early growth of extrusions and intrusions in 316L steel fatigued at room temperature

J. Man[a,*], P. Klapetek[b], O. Man[c], A. Weidner[d]†, K. Obrtlík[a] and J. Polák[a]

[a]*Institute of Physics of Materials, AS CR, Žižkova 22, 616 62 Brno, Czech Republic*

[b]*Czech Metrology Institute, Okružní 31, 638 00 Brno, Czech Republic*

[c]*Institute of Materials Science and Engineering, Brno University of Technology, Technická 2, 616 69 Brno, Czech Republic*

[d]*Institute of Structural Physics, Technical University of Dresden, 01062 Dresden, Germany*

(*Received 28 November 2008; final version received xx*)

Early stages of surface relief evolution of persistent slip markings (PSMs), formed in areas where persistent slip bands (PSBs) intersect the free surface, in polycrystalline 316L stainless steel cycled with constant plastic strain amplitude were studied using atomic force microscopy (AFM) and electron backscattering diffraction (EBSD). Focused ion beam (FIB) technique was employed for obtaining additional, more detailed information on the shape of PSMs. In order to reveal true qualitative and quantitative information about the simultaneous growth of intrusions and extrusions within individual PSMs, identical areas both on the specimen surface and on its inverse copy obtained via plastic replica were studied using AFM. Intrusions are preceded by extrusions regardless of orientation of individual grains of the polycrystal. The first intrusions appear largely around 1% of fatigue life at the moment when "static" extrusions are developed. They appear predominantly but not exclusively at the side of extrusions where the emerging active slip plane is inclined to the surface at an acute angle. They grow faster in comparison with the stage of stable extrusion growth. Typical morphology of mature PSMs developed at 15% of fatigue life consists of ribbon-like extrusions accompanied by two thin parallel intrusions along both PSB/matrix interfaces. Experimental data on the morphology and the growth of extrusions and intrusions are discussed in relation with the theoretical models and computer simulations of surface relief evolution leading to fatigue crack initiation.

Keywords: 316L steel; fatigue; AFM; EBSD; FIB; persistent slip band; persistent slip marking; extrusion; intrusion

1. Introduction

*Corresponding author. Email: man@ipm.cz

†Present address: Institute of Material Science, Technische Universität Bergakademie Freiberg, Gustav-Zeuner-Str. 5, 09596 Freiberg, Germany

Pronounced surface relief formed on the surface of cyclically strained crystalline materials attracts interest of scientists for more than 100 years because it represents the first signs of fatigue damage leading to the initiation of fatigue cracks. The first systematic observation of surface changes produced by cyclic loading was performed by Ewing and Humfrey in 1903 [1]. They used optical microscopy to reveal localized surface damage in the bands of intensive slip, much later called persistent slip bands (PSBs). In addition to this finding they identified the slip bands as incipient crack sites and activated thus hitherto persisting interest in PSB phenomenon.

The localization of the cyclic plastic strain in PSBs followed by the formation of pronounced surface relief (called persistent slip markings (PSMs)) is nowadays accepted as a general and very important feature of cyclic straining in crystalline materials. PSMs arise in areas where PSB lamellae, running parallel to low index crystallographic planes, crop up on the originally flat surface. PSMs consist of local elevations and depressions of the surface known as surface extrusions and intrusions, respectively [2]. Although it is generally agreed that fatigue cracks start to nucleate within PSMs (compare e.g. [3–9]), the exact mechanism of fatigue crack nucleation has not been clarified completely yet. Detailed review of theoretical models and computational simulations of surface relief evolution leading to fatigue crack initiation and their comparison with accessible relevant experimental data on the surface relief in both single- and polycrystals presented in part 1 of the present paper [2] shows only partial understanding of the subject.

Historically, the advancement of our knowledge on the surface relief of PSMs and early damage evolution in fatigue is closely related to the level of experimental technique. Although many different sophisticated experimental techniques based on optical microscopy (OM), transmission electron microscopy (TEM) and scanning electron microscopy (SEM) have been introduced for the study of early fatigue damage during past 50 years (their chronological inventory is given in [2]), most of them could be effectively applied to qualitative and quantitative systematic study of PSMs only in single crystals. Experimental data on the growth of extrusions and intrusions in polycrystalline materials have been thus scarce for a long time.

A revolution in quantitative study of surface features in strained and cyclically strained materials has been initiated by the advent of atomic force microscopy (AFM) in the early 1990s. AFM was firstly utilized in fatigue by Harvey et al. [10] to obtain quantitative information about the slip spacing and slip height displacements in cyclically loaded polycrystalline titanium and high strength-low alloy (HSLA) steel. True PSMs consisting of

extrusions were observed by AFM in a structural steel for ships later by Nakai et al. [11]. Intrusions were firstly revealed by AFM using plastic replicas also by Nakai et al. [12].

Nowadays, AFM is accepted to be the most powerful microscopic technique used for accurate study of the surface topography of PSMs and its evolution. It has been applied mainly to simple f.c.c. polycrystals fatigued at room temperature both directly on metallic specimens (copper [13–17], 316L steel [13,18–22] and α-brass [23]) and using plastic replicas (α-brass [12,24] and 316L steel [25]). Less numerous observations have been reported for fatigued b.c.c. metals [21,26–30]. Only limited data are available for polycrystalline nickel-base superalloys fatigued at room [31–33] and elevated [31] temperatures and quite recently for a duplex (A+F) stainless steel [34,35].

Experimental results on the growth of PSMs obtained during the last decade by AFM in fatigued polycrystals can be briefly summarized as follows. The growth of intrusions was studied by Nakai and his co-workers in a fine [12, 24] and coarse [24] grained α-brass fatigued in cyclic plane bending with different stress amplitudes. They reported a linear growth of intrusion depth with the logarithm of the number of cycles and 'drastic' increase in the depth of intrusions which is interpreted as the outgrowth of an intrusion to a crack [12, 24]. Based purely on a simple geometrical model for ideally oriented slip system they deduced that the critical value of the intrusion depth in the direction of active Burgers vector at the moment of crack initiation is 380 nm, independent of the inclination of PSM relative to the stress axis, the stress amplitude and the grain size [24]. Similar conclusion was drawn by Wang et al. from their more thorough AFM and electron backscattering diffraction (EBSD) study of intrusion growth in 316L steel cyclically strained in torsion [25]. They suggest that instead of the intrusion depth in the direction of active Burgers vector its component perpendicular to the surface trace of a PSM or simply the intrusion depth should be used as the criterion of a crack initiation. Critical value of both characteristics was found to be about 170 nm [25].

Growth of extrusions was studied by Man et al. in 316L austenitic stainless steel [20, 21] and in ferritic stainless steel [21, 29] fatigued with constant plastic strain amplitude. For both steels it was found that the height of extrusions increases quickly at the onset of cycling and later approximately linearly with the number of cycles up to the end of fatigue life. Abe et al. [28] studied the growth of extrusions in ferritic-pearlitic low carbon steel alloyed with Ni, Si or Cu cyclically loaded in out-of-plane bending. They found similar results: extrusions grow quickly during the initial stage and then their growth rate decreases or saturates.

Systematic growth of extrusions was reported for both phases in a duplex (A+F) stainless steel by Salazar et al. [34,35]. Whereas linear growth of extrusions was observed in case of austenitic phase, a tendency for saturation of extrusion growth was apparent for ferritic phase. Only limited experimental data on the growth of the average extrusion height are available for copper [14] and Ni-base superalloy polycrystals [32].

With respect to the methodology of AFM observations it is very important to note that till now the growth of extrusions and intrusions has been monitored either directly on the specimen surface [14,17,20,21,27–29,32,34,35] or using plastic replicas [12,24,25]. Although it was unambiguously documented that AFM has some limitations in observations of PSM topography [19,21,36] and in quantitative assessment of the extrusion-intrusion pairs [21,36] a systematic study using both observations (specimen and replica) in order to obtain true quantitative data on simultaneous growth of extrusions and intrusions in an individual PSM has not been performed so far.

In this work an extensive and systematic study of the early stages of the surface relief evolution in polycrystalline 316L steel[1] fatigued with constant plastic strain amplitude at room temperature using AFM with respect to the crystallographic orientation of individual grains determined by electron backscattering diffraction (EBSD) is reported. In agreement with the given limitations of AFM, extrusion growth was systematically monitored by direct observation of the metallic surface and plastic replica technique has been used to reveal intrusions in identical areas of the specimen surface. Profiles of the surface relief topography were additionally studied in cross-sections produced by the local milling using focused ion beam (FIB) technique. Qualitative and quantitative data on the morphology of individual PSMs and its evolution during cycling and on the growth of intrusions and extrusions with respect to the orientation of individual grains of polycrystals are reported. Experimental results obtained are used to construct a detailed scheme of the surface relief formation. They are compared with previous results and discussed in relation to recent theoretical models and computer simulations of surface relief evolution leading to fatigue crack initiation (for comparison of the present experimental data with theoretical model see also part 1 [2]). Some preliminary results on this subject have been already published elsewhere [37,38].

2. Experimental details

[1] Polycrystalline 316L stainless steel is very suitable candidate for such studies from many aspects. It teeters on the transition from wavy slip to planar slip and thus its surface relief topography is not as complicated as in the case of copper. Owing to its corrosion resistance it is predestined for tedious, time-consuming systematic AFM observations.

2.1. *Material, specimens and fatigue tests*

Austenitic 316L stainless steel was supplied by Uddeholm (Sweden) in the form of a 25 mm thick plate with the following chemical composition (in wt. %): 0.018 C, 0.42 Si, 1.68 Mn, 0.015 P, 0.001 S, 17.6 Cr, 13.8 Ni, 2.6 Mo, rest Fe. The heat treatment, consisting of solution annealing at 1080 °C and water quenching, resulted in an average grain size of 39 μm (found using linear intercept method without counting twin boundaries).

Cylindrical specimens with threaded ends had a gauge diameter and length of 8 and 12 mm, respectively. A shallow notch in the form of a concave facet having approximately elliptical shape (for details see ref. [18, 20]) was produced in the centre of the specimen to facilitate the observation of the surface relief evolution and fatigue crack initiation. Specimens were annealed at 600 °C for 1h in vacuum. The notch area was mechanically and electrolytically polished. For easier orientation on the specimen surface some fine circular marks 400 μm in diameter were engraved in the central part of the polished notch before cycling.

The specimens were cyclically deformed in symmetrical push-pull in a MTS computer-controlled servohydraulic testing machine at room temperature in air under strain control. Desired plastic strain amplitude was applied since the first quarter of the loading cycle using a set MTS-BASIC programs developed in our laboratory (for details see ref. [39]). Plastic strain amplitude $\varepsilon_{ap} = 1\times10^{-3}$, derived from the half-width of the hysteresis loop, and the total strain rate $\dot{\varepsilon} = 1.5\times10^{-3}$ s^{-1} were kept constant for the whole period of the fatigue test. The cycling was periodically interrupted at cycle numbers corresponding approximately to a geometric series and the specimen was removed from the testing machine both for the replication and the observation of the specimen surface (see figure 1).

[Insert figure 1 about here]

2.2. *Microscopic observation and replication procedure*

The detailed study of surface topography changes during cyclic straining was performed using the Accurex IIL atomic force microscope (Topometrix, USA). Contact imaging mode in air was used to obtain constant-force topographic images. A V-shaped silicon nitride cantilever with a sharpened pyramidal tip having the radius of curvature of 20 nm and the vertex angle 36° was applied. Observations on plastic replicas were made mostly with a standard

pyramidal tip whose radius of curvature was 50 nm and the minimum and maximum vertex angle was 53.1° and 70.5° respectively (for the scheme of its geometry see ref. [21]).

Two basic scan sizes were chosen. AFM scans 100×100 μm^2 with 400×400 data points were used for qualitative analysis and an overall evaluation of slip activity within individual grains (the detection of active slip systems). For the detection of intrusions and quantitative evaluation of extrusion and intrusion growth smaller areas 15×15 μm^2 with 500×500 data points were captured. The surface profiles of extrusions and intrusions within individual PSMs were determined using the implemented software.

An optical microscope ZEISS Neophot 32 with a CCD camera was used for the first inspection of specimen surface, pre-selection of grains for systematic AFM study and quick checking of quality of the plastic replicas. Some additional examinations of the specimen surface were performed using a JEOL JSM-6460 SEM.

Replication procedure steps were the following. Before each replication and AFM specimen observation the specimen surface was carefully cleaned in acetone and subsequently in pure ethanol in ultrasonic cleaner. Celluloid film of 0.09 mm in thickness was softened with a solution of 50% acetone and 50% amyl acetate and applied to the specimen surface. In order to keep the same fluidity conditions and good fidelity of replicas each film was pressed down to the specimen surface during initial stage of drying. Once the replica was thoroughly dried (after about 8 hours), double-sided adhesive tape of proper size was gently put onto the back of the replica. The tape-replica assembly was then lifted from the specimen and mounted to the stub holder by using the exposed double-sided tape.

2.3. *Crystallographic orientation of surface grains*

The crystallographic orientations of individual grains were determined in the scanning electron microscope using electron backscattering diffraction (EBSD) method. The EBSD measurements were carried out after the termination of fatigue tests (N = 6 750 cycles). The orientation imaging microscopy (OIM) system TSL DC 3.5 installed on SEM Philips XL 30 at BUT Brno was mostly used. Additional EBSD measurements were performed on the SEM at TU Dresden (Zeiss DSM 962) with an EBSD detector and the Channel5 software from HKL.

The EBSD (pseudo-Kikuchi) patterns were analyzed and orientation matrices $\mathbf{g}_{ij}$ with respect to the specimen orthogonal co-ordinate system for each grain were obtained. Figure 2

shows the position of the stress axis of all 32 surface grains plotted in the standard stereographic triangle. It is apparent that no specific grain orientation was preferred.

[Insert figure 2 about here]

Using $\mathbf{g}_{ij}$ matrices the Schmid factor μ for each of the 12 possible {111} ⟨110⟩ slip systems and the slip plane traces (i.e. intersections of a slip plane with the specimen surface) were calculated. Comparison of the observed and calculated angles of PSMs with the stress axis in individual grains allows unambiguous identification of the active slip plane. In general, there is a great difference in Schmid factors among different slip systems in the same slip plane, therefore the active slip direction was chosen so that the respective slip system was characterized by the highest Schmid factor.

The inclination of active slip plane relative to the specimen surface in each grain is characterized by the angles β_1 and φ as shown schematically in figure 3 for two PSMs on the specimen surface. Angle α between the Burgers vector **b** of active dislocations and the specimen surface and angle β between the slip plane normal and the specimen surface were computed as well. The values of these angles for all 32 surface grains together with identified slip systems and other crystallographic characteristics are listed in table 1.

[Insert figure 3 about here]

[Insert table 1 about here]

2.4. *Cross-sectioning of PSMs using focused ion beam technique*

Surface relief topography of PSMs in specimens, cycled under the identical conditions described above, was studied also on cross-sections produced by local milling using the focused ion beam (FIB) technique. Sections perpendicular both to the specimen surface and PSMs were prepared by a FIB system FEI Quanta 3D after 500 cycles. After applying additional 1500 cycles the resulting surface relief was examined by the high resolution field emission gun SEM (SEM-FEG) (FEI Quanta FEG). Further details concerning the FIB cross-section procedure can be found elsewhere [40].

3. Results

3.1. *Assessment of overall cyclic slip activity evolution*

The AFM study of the surface relief evolution in 316L steel cycled with constant plastic strain amplitude 1×10^{-3} has revealed that PSMs could be detected already after 10 cycles. After the identification of slip systems in individual grains (see table 1) statistical evaluation of the slip activity was performed. Figure 4 documents the evolution of slip activity within all 32 surface grains with the number of cycles. In the majority of grains only one slip system was activated after 10 cycles; 4 grains were without any PSMs at this cycle number. With further cycling the number of grains with two active slip systems (primary and secondary, P+S) gradually increases and at the same time the number of grains without PSMs decreases. The number of grains with different slip activities stabilized after 500 cycles and at the moment of termination of the fatigue test (N = 6750 cycles ~ 15% N_f) one slip system was active in 20 grains, two slip systems in 11 grains and only in 1 grain no PSMs were present.

[Insert figure 4 about here]

Concerning the spatial distribution of PSMs, a characteristic difference between grains with activated one or two slip systems was generally found. PSMs in grains in which one slip system has been activated (P or S – see table 1) were evenly distributed whereas the average inter-PSM spacing varied from grain to grain. In grains with two activated slip systems it is true only for PSMs corresponding to the primary slip system. PSMs corresponding to the secondary slip system (S_1 or S_2 – see table 1) were developed only locally, typically in the close proximity of a grain boundary.

3.2. *Characteristic features of surface relief evolution*

Characteristic sequences of the early evolution of the surface relief topography are documented by AFM micrographs shown in figures 5 and 6, obtained by direct specimen observation and using plastic replicas, respectively.

[Insert figure 5 about here]

The series of AFM micrographs in figure 5 shows the evolution of the surface relief in grain No. 62. The same position on all micrographs is indicated by the small black arrow. This grain with high Schmid factor μ_p = 0.49 is oriented nearly for single slip (orientation factor Q = 0.925 [41] – see table 1) and thus only primary slip system (111) [$\bar{1}$01] has been activated in this grain. Dense set of parallel, nearly equidistantly spaced fine slip markings (slip lines) with an average separation distance of 0.8–0.9 μm can be seen at the very early

stage of cycling (see slip markings numbered 1 to 21 for $N = 10$ in figure 5(a)). To accentuate their contrast and to visualize these fine slip markings (SMs) all AFM micrographs are displayed in the shadowed format. Most of the fine SMs traverse the whole grain surface and only some are fragmentally developed. They are characterized by compressive slip steps (see the next section) with a typical height 4–12 nm. Their height and density do not change with increasing number of cycles, however, cyclic slip activity within some of them becomes persistent – see PSMs 4, 7 and 10 in figure 5(b). The persistency of localized cyclic slip is clearly manifested by gradual development of hilly ribbon-like extrusions in these PSMs. The growth of extrusion height and width is clearly apparent from the sequence of PSM profiles presented in the next section. In order to differentiate distinctly the true PSMs from the fine SMs observed in the very early stage of fatigue life their numbers are highlighted by encircling in figures 5(b) to 5(f). With further cycling the number of true PSMs increased successively and stabilized in this grain after 100 cycles (0.2% N_f) (cf. figures 5(b) and 5(c)). Only about 50% of SMs observed after 10 cycles become PSMs in this grain and the extrusions grew continuously up to the end of the fatigue test (results on persistency for all grains are given in the next section). Note that some PSMs were nucleated in the centre of a grain and with continuing cycling they extended up to the grain boundary (cf. PSM 10 in figures 5(c) and 5(f)).

Further specific features of surface relief evolution which could be revealed by AFM using plastic replicas only are apparent from figure 6. The AFM micrographs of plastic replicas in figure 6 show the surface relief evolution within the identical area of grain No. 78 at selected number of cycles. The same position in all AFM micrographs is indicated by the small white arrow. Grain No. 78 is oriented for double slip (see figure 2 and table 1) and thus two slip systems were activated in this grain. Figure 6 shows PSMs corresponding to the primary slip system $(111)[\bar{1}01]$. They traverse almost the whole grain and are separated by the non-deformed surface with an average inter-PSM spacing of around 3.5 μm. Very faint PSMs corresponding to the secondary slip system $(\bar{1}11)\,[101]$ were produced solely close to the grain boundary and they are not imaged here.

[Insert figure 6 about here]

At the beginning of cycling (N = 350 cycles) PSMs consist only of ribbon-like extrusions (see figure 6(a)). The first intrusions running parallel to extrusions were detected in this grain after 500 cycles – see the most developed PSMs 1 and 3 in figure 6(b) – at the side

of the extrusion where the emerging active slip plane is inclined to the surface at an acute angle (side B in figure 3). They are very fine and thin in comparison with extrusions; their depth is typically only 10 nm at this stage of fatigue life. With further cycling they grow and, moreover, another intrusions appear (some of them only locally) as indicated in figure 6(c). After 2000 cycles (4.3% N_f) each extrusion is accompanied by one (PSM 4 in figure 6(d)) or two (PSMs 1, 2 and 3) parallel intrusions the depth of which can fluctuate along PSM.

3.3. *The 'persistency' of localized cyclic slip*

The series of AFM micrographs documenting the gradual development of PSMs similar to figures 5 and 6 were obtained for all relevant 31 grains. Careful comparison of AFM micrographs (surface area 15×15 μm^2 for smaller grains, 15×15 μm^2 and 50×50 μm^2 for larger grains) and the analysis of the corresponding surface relief profiles allowed to determine the above mentioned 'persistency' of localized cyclic slip in a grain. In several cases some fine SMs at the later stages are not clearly visible from these AFM micrographs (cf. figures 5(d), 5(e) and 5(f)) and thus they seem to 'disappear' during cycling. Checking the respective surface relief profiles, however, it can be showed that these SMs with constant slip step height are permanently present within a grain (i.e. they are irreversible). This is clearly demonstrated in figure 7 which shows surface relief profiles obtained at different stages of fatigue life in the identical cross-section perpendicular to the direction of PSMs in the grain 62; its position is apparent from figure 5(e). Note that the vertical scale (i.e. the height scale in the *z*-direction) in figure 7(a) is exaggerated by a factor of 6 with respect to the horizontal scale (i.e. the lateral scale in the *x*-direction) to visualize small slip steps corresponding to fine SMs. For comparison, the profiles obtained at the identical location for 3000 and 6750 cycles are shown in the one-to-one scale in figure 7(b) with indicated slip plane inclination (see table 1). In this case the angular values can be read directly from the figure, however, fine SMs become nearly invisible.

[Insert figure 7 about here]

As it is apparent from figure 7 only compressive slip steps (cf. figures 7(a) and 7(b)) corresponding to fine SMs 7, 9 and 10 were present in this grain after 10 cycles. While their height ranging from 8–12 nm did not change with further cycling, the fine SMs 7 and 10 became areas of permanent slip activity as is clearly evidenced by systematically growing extrusions (see PSMs 7 and 10 in figure 7). Slip steps with approximately similar height (5–

20 nm) that was constant during the whole cycling were found also in other grains. Both compressive and tensile slip steps were detected but all slip steps within an individual grain had the same sign.

The persistency of localized cyclic slip, denoted as p_s, was quantitatively evaluated for all 31 grains at the end of fatigue test. The persistency p_s is defined as the ratio of the number of true PSMs (with gradually growing extrusions and later intrusions) recorded at the end of fatigue test ($N = 6750$) to the number of fine SMs detected early in the fatigue life ($10 \leq N \leq 1000$). The results are presented in figure 8. The data on persistency for other stages of the fatigue life are not presented here, but generally, p_s in individual grains was found to be increasing with increasing number of cycles. Data on PSMs corresponding to the secondary slip systems activated in the proximity of a grain boundary in grains with two active slip systems are not included into the data sets; the evolution of their topography, however, has the same characteristic features as those found for the primary slip system. The typical number of SMs or PSMs evaluated in each grain was 12–20; a lower number of SMs or PSMs (4 to 8) has developed and was assessed in a few grains (grains 55, 61, 65 and 72). As it is apparent from figure 8, the persistency of localized cyclic slip after 6750 cycles can vary among individual grains in the interval between 15 and 100%. However, in the majority of grains its value is typically about 80–100%; for 55% of surface grains p_s is in the interval of 90–100%.

[Insert figure 8 about here]

3.4. *Crystallographic aspects of PSM morphology evolution: statistics*

To obtain more detailed information about crystallographic features of PSMs, the specific morphology of extrusion-intrusion pairs (EIPs) were correlated with the inclination of the active slip plane to the surface in individual grains (see figure 3). In spite of the variability of PSM morphology, four typical configurations of EIPs were identified during careful scrutiny of more than 280 AFM micrographs (15×15 μm^2) taken at different stages of fatigue life from plastic replicas. They are schematically illustrated in figure 9. PSM morphology denoted "A" ("B") consists of an extrusion and one intrusion produced at the side of the extrusion where the emerging active slip plane is inclined to the surface at an obtuse (acute) angle (cf. figures 3 and 9). PSM type "A+B" consists of a central extrusion accompanied by two intrusions running alternatively along both sides A and B. PSM type "A/B" consists of a central extrusion accompanied by two parallel intrusions going simultaneously along its both sides.

In addition to the EIP morphology shown in figure 9 isolated intrusions, unaccompanied by parallel extrusions, were also detected. They were reported also by other authors [42–46]. Our observations however showed that in reality these intrusions were isolated only locally along the intersection of a PSB with the specimen surface, typically at the end of a PSM and the remaining part of the same PSM always comprised an extrusion, accompanied later in fatigue life by one or two parallel intrusions. It should be stressed that these "isolated" intrusions are certainly not a general and dominant feature of PSM topography; they were detected very rarely, only in several PSMs, and thus they were not considered in the following statistical treatment of the evolution of PSM topography.

[Insert figure 9 about here]

Statistical treatment of the overall evolution of PSMs with respect to the morphology mentioned above is presented in figure 10. The histogram comprises experimental data on 197 PSMs within identical areas in 31 individual grains. They were obtained by careful evaluation of more than 350 AFM micrographs (15×15 μm^2) taken at different stages of fatigue life directly from the specimen surface and simultaneously using plastic replicas. It should be stressed that only the data on PSMs which became really persistent (see above) were included in statistical treatment.

[Insert figure 10 about here]

It is apparent from figure 10 that not all tracked PSMs were detected immediately from the onset of cycling. Their number slowly increases with increasing number of cycles until saturation around 1000 cycles. The most important findings concerning the evolution of PSM topography can be summarized as follows: (i) at the very early stage of cycling ($N = 10$) mostly fine SMs with slip step topography are present in the sites where the true PSMs develop later, (ii) with the continuing cycling the number of PSMs comprising purely extrusions decreases and at the same time the number of PSMs consisting of both extrusions and intrusions gradually increases, (iii) an intrusion developing at the PSB/matrix interface is preceded by an extrusion regardless of the orientation of individual grain of a polycrystal and (iv) already after 2000 cycles (~ 4.3% N_f) more than 96% of extrusions are accompanied by two or at least one parallel intrusion.

Figure 11 shows another important result derived from the experimental data. Similarly to figure 10, PSMs are sorted according to PSM types as indicated in figure 9.

However, each of all 197 PSMs is now counted only once, namely at the moment when the first intrusion appeared within the respective PSM. It is apparent from this figure that intrusions appear very early in fatigue life. The majority of the first intrusions were detected after 100–2000 cycles (~0.2–4.3% N_f), much more frequently at the side B, i.e. at the side of an extrusion where the emerging active slip plane is inclined to the surface at an acute angle (see figure 3).

[Insert figure 11 about here]

3.5. *Shape of extrusions and intrusions*

Careful evaluation of profiles of many PSMs in variously oriented individual grains obtained by AFM both on the metal surface and via plastic replica at different number of cycles shows that the shape of extrusions and intrusions evolves in a characteristic way.

Most characteristic features of the development of extrusions are apparent from figure 7. The first, very small embryonic extrusions with a hill-like geometry were detected after 50 cycles in the grain No. 62 – see figure 7(a) (in some other grains already after 10 cycles). The profiles of both embryonic extrusions overlay the profile of the fine slip steps developed before and suggest thus that the fine SMs demarcate the embryos of future PSBs. With further cycling ribbon-like extrusions widen and heighten and after 3000 cycles they acquire a characteristic triangular profile (cf. figures 7(a) and 7(b) which show the same profile at different scales) whose asymmetry can be directly related to the inclination of the active slip plane to the surface, as indicated in figure 7(b). Comparing figures 7(a) and 7(b) it is clear that extrusions widened about three-times. Moreover, using the SM 9 as a reference mark it can be seen that while the widening of PSM 10 was approximately symmetrical, in case of PSM 7 it was asymmetrical.

With additional cycling the extrusions, appertaining to PSMs 7 and 10, continue in their growth. After 6750 cycles well developed extrusions display more or less rounded profile, which is rugged on the top (see PSM 10 in figure 7). Measured profile of both extrusions is already laterally distorted at this stage. However, their height is not affected by the AFM tip and thus true experimental data on the extrusion growth can be obtained [21, 36]. Considering the shape of AFM tip and the theoretical inclination of the active slip plane in the grain 62 (β = 58.8°) indicated in figure 7(b), it is apparent that only the side A of both extrusions could be recorded truly. In addition it can be clearly seen that the slope at the bottom of both extrusions is identical to the computed slip plane inclination, i.e. the flat lateral

surface at the bottom of the extrusions corresponds to the (111) slip plane found for this grain (see table 1). Similar measurements, performed for the well-developed extrusions also in other differently oriented grains where the inclination could be assessed (cf. the AFM tip geometry shown in figure 7(b) and the theoretical slip plane inclination in table 1) yielded the same results.

The sequence of profiles of PSMs obtained by AFM on plastic replicas, documenting the growth of intrusions similar to that shown in figure 7, is not presented here. Nevertheless, several important features could be revealed by their inspection. The thickness of intrusions at very early stage of cycling was found to be typically 80–100 nm, which represents only 1/4 or less of the thickness of appertaining parallel extrusions. Profile measurements of developed intrusions in grains where the inclination could be assessed (see above) showed that intrusions grow in the active slip plane direction and thus the shape of intrusions in this stage is always laterally distorted. Only one side of each intrusion developed at both sides of an extrusion from plastic replicas is evaluated faithfully (cf. figure 3 and figure 9 in [21]): it is the side of an intrusion at position B whose normal is directed to the matrix and the side of an intrusion at position A whose normal is directed to the PSB.

To obtain a more comprehensive view on the PSM topography and to reveal a true geometry of extrusions and intrusions some additional observations were made with the help of local milling by the FIB technique. An example obtained with this technique is shown in figure 12. This figure shows high resolution SEM-FEG micrograph of a cross-sectioned individual PSM in 316L steel cycled with constant $\varepsilon_{ap} = 1\times10^{-3}$. The cross-section was produced after 500 cycles and then additional 1500 cycles were applied. Afterwards the area of the specimen surface and the cross-section plane was photographed without any further FIB repolishing to keep relatively sharp contours conceived by the additional cycling. They can be seen on the roughened surface of the cross-section plane, probably due to the fact that the active Burgers vector is not exactly parallel with it. This roughening is observable only within the area of continuing slip activity, i.e. within the area where PSB lamella intersects the cross-section plane, while the surface corresponding to the matrix on the cross-section plane remained smooth.

[Insert figure 12 about here]

The well-developed PSM inclined to the specimen surface approximately at 70° consists of extrusion and a small intrusion at its left side (side A in figure 3). Whereas the

thickness of the extrusion is about 500 nm, the thickness of accompanying intrusion is much smaller. The top of the extrusion is not smooth but displays gently rugged surface morphology. Both sides of extrusion have the same slope, which perfectly matches with the roughened area on the cross-section plane, i.e. with the appertaining PSB. Another small extrusion developed to the left from the larger original extrusion.

3.6. *Quantitative evaluation of extrusion and intrusion growth*

Quantitative data on the growth of extrusions and intrusions were obtained from the profiles of individual PSMs in selected sections. In agreement with our previous studies on surface relief and its evolution in 316L steel [20] the sections were taken perpendicular both to the grain surface and to the direction of the PSM on the surface. For the evaluation of the extrusion growth on the specimen surface and of the intrusion growth on the plastic replicas it was very important to choose the PSM cross-sections in individual AFM micrographs always in the same location. In this way the simultaneous growth of extrusions and intrusions in one grain was obtained.

Only early stages of intrusion formation could be documented reliably since intrusions are very thin and deep and the plastic replica reproduces their shape only when their depth is less than 0.5 μm, exceptionally up to 1 μm. For deeper intrusions several artefacts coming from the specific geometry of EIPs and the limits of replica technique were repeatedly observed: (i) an intrusion growing faster at the side B hides a small intrusion at the side A on the replica surface (see the schematic inset in figure 13(b)), (ii) large intrusions can be bent towards the replica surface and (iii) during stripping out the replicating film from the deep intrusions part of the film remains in the intrusion and also a well-developed extrusion can be broken and taken away from the specimen surface with replicating film. The appearance of all these artifacts should be kept in mind in the interpretation of the results obtained with the use of plastic replica technique for the quantitative evaluation of intrusion growth. The profiles of intrusions, displayed in the scale one-to-one, should be carefully checked to avoid misleading conclusions.

An example of the kinetics of extrusion and intrusion growth in the early stages of fatigue life is shown in figure 13. The plots correspond to two most frequent configurations of extrusion-intrusion pairs observed i.e. types “A+B” and “B” indicated in figure 9. In both grains the extrusions start to grow first, and only after some delay an intrusion develops and grows with higher growth rate. Figure 13(a) corresponds to one intrusion developed at the

side of extrusion where the angle between the extrusion and the surface was acute (PSM type "B" in figure 9). In this case the growth rate of the intrusion is nearly five times higher than the growth rate of the extrusion. When two intrusions develop (figure 13(b)), the growth rate of intrusions is only slightly larger than the growth rate of the extrusion. The first intrusion appears at the position B (cf. figures 13(b) and 9) and much later second intrusion starts growing at the position A. The growth rates of both intrusions are approximately identical.

[Insert figure 13 about here]

4. Discussion

4.1. *Development of overall slip activity and activated slip systems*

Systematic AFM study of surface relief evolution within individual grains of polycrystalline 316L steel cycled with constant plastic strain amplitude of 1×10^{-3} has revealed very early localization of the cyclic plastic strain. Fine SMs and in some cases also true PSMs corresponding to primary slip system were detected in majority of grains already after 10 cycles. With further cycling the plastic deformation is accommodated mostly by one slip system accompanied by gradual increase in the number of intensifying PSMs (see figure 10), developing in the sites of former fine slip markings. PSMs in these grains were generally found to be evenly distributed with an average inter-PSM spacing varying from grain to grain.

Two activated slip systems were present in one third of grains investigated after 500 cycles (see figure 4). PSMs gradually developed from fine SMs corresponding to the secondary activated slip system were, however, found in great majority of grains only locally, in the vicinity of the grain boundary. The secondary PSMs developed more frequently in grains oriented for double and multiple slip (i.e. with the loading axis lying close to the borders or corners of the standard stereographic triangle.

The results on slip activities obtained in relatively small number of individual grains agree with those obtained previously in much more extensive study of coarse-grained 316L steel [18]. In comparison with previous results higher frequency of grains with two activated slip systems has been detected even after small number of cycles (cf. figure 4 and table 1 in [18]). This difference could be attributed to the finer grain size of 316L steel used in the present study.

Only one grain (No. 73) remained after 6750 cycles without detectable PSMs. Blochwitz et al. [47] introduced two criteria to explain the absence of PSMs: (i) normal

component of the Burgers vector (the component which is perpendicular to the specimen surface) is small (s_z<0.15) or (ii) the Schmid factor of the primary slip system is low (μ_p<0.43). Both 'invisibility' criteria for grain No. 73 ($s_z = \sin\alpha = 0.17$, μ_p=0.455 – see table 1) are nearly met. Another possible explanation has been outlined recently by Sauzay and Jourdan [48] and Sauzay [49] who evaluated the effect of crystalline elasticity and neighboring grain orientations on the stress state of a favorably oriented grain using Monte-Carlo finite element computations. They found that the critical shear stress for PSB formation can be changed in dependence on the neighbor grain orientation. Sauzay and Man [50] showed for some grains without PSMs that in the dependence on the size and the orientation of neighbor grains the 'effective' Schmid factor could be reduced by 24% relative to the 'classical' Schmid factor obtained by EBSD; its value was assessed using the cumulated probability of the Schmid factor given in [49] to about 0.34.

4.2. *Fine SMs, PSB nucleation and its relation to cyclic stress-strain response*

The very early formation of fine SMs and the appearance of the first true PSMs, manifesting the cyclic strain localization into PSBs, correspond to the evolution of the stress amplitude σ_a and the loop shape parameter V_H shown in figure 14. The loop shape parameter [51] is equal to the ratio of the area of the hysteresis loop and the area of circumscribed parallelogram, i.e.

$$V_H = \frac{\oint \sigma \mathrm{d}\varepsilon}{4\sigma_a \varepsilon_{ap}}. \qquad (1)$$

[Insert figure 14 about here]

The short period of cyclic hardening during which mostly fine SMs are formed is followed by the achievement of maximum stress amplitude and slow cyclic softening until the end of fatigue life. The loop shape parameter V_H decreases and reaches the local minimum approximately at the cycle number when the stress amplitude reaches its maximum. The appearance of the first true PSMs found by AFM on the specimen surface during 10–50 cycles correlates very well with the local minimum of V_H (see figure 14). In analogy with simple fcc single- and polycrystal behavior (for review see [8, 46]) the minimum of V_H can be regarded as the onset of cyclic strain localization into the PSBs also for the present material. Similar results concerning the characteristic changes of the hysteresis loop shape reflecting the start of cyclic slip localization were obtained recently for austenitic stainless steel single- [52] and polycrystals [20] and for ferritic stainless steel [29].

In agreement with our previous study [20] the present results show that the height and the sense of fine SMs do not change with continuing cycling. Moreover, most of them became areas of permanent slip activity manifested by gradually growing PSMs (see figure 8). Similar results on the persistency of localized cyclic slip were found by Salazar et al. for austenitic phase in a duplex stainless steel [34]. These findings together with the fact that the small embryonic extrusions arise exactly at the locations of fine SMs (see figure 7) indicate a possible mechanism of PSB formation in surface grains of a polycrystal. The experimental data concerning this topic and their discussion are however beyond the scope of the present paper and will be presented in detail in separate publication [53].

AFM detection of fine SMs at the onset of cycling is in agreement with previous studies. Hunsche and Neumann [54] studied surface relief profiles in fatigued copper single crystals using a section micromilling technique in the SEM and they noticed compressive as well as tensile slip steps present at the early stage of cycling of copper crystals at those locations where hilly extrusions develop later. Very small slip offsets are apparent also from surface profiles of young individual PSMs in copper single crystal obtained earlier by Mughrabi et al. using the SEM contamination-line technique [43]. Although it was not explicitly mentioned by the authors, slightly different matrix height level at both sides of PSMs clearly shows the evidence of a very fine compressive slip step hidden in an extrusion developed during 500 cycles (cf. figure 7 in [43] and figure 7(a)). Similar fine SMs with slip step height of about 8 nm were detected after 20 cycles in most of the grains of a 316L austenitic stainless steel fatigued in vacuum with $\varepsilon_{ap} = 2\times10^{-3}$ also by Villechaise [22]. Salazar et al. [34,35] reported for the austenitic phase of a duplex stainless steel cyclically strained with $\varepsilon_a = 8\times10^{-3}$ the presence of straight slip lines resembling unidirectional steps (i.e. fine SMs) with a mean height of 10–20 nm which were in some cases already after 5 cycles accompanied by extrusions, growing along these slip lines.

4.3. *Evolution of surface relief topography of PSMs*

Detailed study of the morphology of a great number of individual PSMs and the systematic monitoring of their evolution during the early stages of fatigue life revealed that PSM topography evolves in a characteristic way. The identification of specific features of the surface relief topography, the correlation of particular morphology of EIPs with the inclination of the active slip plane in individual grains together with our previous results obtained by AFM and other experimental techniques [18,20,21,29,36,55] allow to construct a

plausible scheme of the early stages of surface relief evolution. This scenario, encompassing all characteristic successive stages of surface relief evolution is illustrated schematically together with the diagram of the kinetics of extrusion and intrusion growth in figure 15. Several pertinent results supporting this scheme can be found also in available literature (see below).

[Insert figure 15 about here]

In agreement with this scheme PSMs start as surface extrusions. The first embryonic extrusions are thin and they can be developed only locally along the intersection of PSB embryos with the specimen surface (see figure 15(a)). With continuing cycling they widen and heighten and approximately after 200–1000 cycles the ribbon-like 'static' extrusions are formed (figure 15(b)). They acquire a smooth, roughly triangular profile whose asymmetry depends on the inclination of PSBs to the specimen surface. Their height in the direction of the active Burgers vector is proportional to the grain size below the specimen surface, as indicated experimental study by Man et al. [18].

After rapid development of ribbon-like static extrusions (stage I in figure 15) they continue in their growth at lower growth rate (see figure 15(e)). Typically after 100 – 2000 cycles (~0.2–4.3% N_f) intrusions start to appear, often only locally, along extrusions, predominantly but not exclusively at the side B where the emerging active slip plane is inclined to the surface at an acute angle (c.f. figures 11, 15(c) and 15(e)). They are four or more times thinner than extrusions and they deepen in the active slip direction. The rate of intrusion growth is higher than that of extrusions and depends on the type of intrusion, e.g. whether one or two parallel intrusions grow simultaneously. Typical morphology of mature PSMs developed after 6750 cycles (~15% N_f) is shown in figure 15(d). It consists of central ribbon-like extrusion accompanied by two thin parallel intrusions going simultaneously along PSB/matrix interfaces the depth of which varies along their lengths much more than the height of extrusions. Well-developed extrusions, protruding from the surface over the whole thickness of PSB lamellae, display more or less rounded profile rugged on the top.

The direct experimental evidence that intrusions are preceded by extrusions irrespective of individual grain orientation found in the present work for 316L steel has not been reported so far. Nevertheless, the limited experimental results obtained for polycrystalline copper fatigued at room temperature [56,57] indicate the same conclusion. Kwon et al. [56] investigated at high resolution shadowed surface replicas taken from the

identical position of the specimen by SEM and they noticed that while only slip bands (i.e. extrusions) are seen after 300 cycles of straining with $\varepsilon_a = 8\times10^{-4}$, small slip band cracks are seen after 500 cycles. Using the 0.1 μm crack depth criterion with SEM examination of replicas they determined the number of cycles to crack initiation and found that this number of cycles increases with decreasing strain amplitude. It indicates that with the decreasing strain amplitude the appearance of the first intrusion is more and more delayed. Kim et al. [57] used the same technique and reported that only faint slip bands (i.e. ribbon-like extrusions) are present in a grain after 100 cycles with $\varepsilon_a = 1.5\times10^{-3}$ but after 5000 cycles the same PSMs consist of extrusions accompanied by one, or more frequently by two, parallel intrusions.

The shape of "young" extrusions was studied in copper single- [43,58,59] and polycrystals [59] fatigued at room temperature using the contamination line technique in the SEM. It was found that "young" extrusions possess a triangular profile and the surface of extrusions is smooth without any detectable surface roughening. These findings are in agreement with the present AFM results and with our results obtained previously [20, 21]. At a later stage the triangular form is lost and the extrusion profile becomes more complex as could be revealed only by viewing the FIB-cross-sections in SEM-FEG – see figure 12. Extrusions show more or less rounded profile which is rugged on the top in good agreement with model by Differt et al. [60]. The magnitude of the mean depth (peak-to-valley) of the roughness profile at the top of the extrusion shown in figure 12 agrees quantitatively with the predictions of this model [43,60]. Similar roughening superimposed on the top of extrusion and corresponding to the random fine slip has been already evidenced by the SEM for copper single crystals [60] and more recently by the high-resolution SEM-FEG also for 316L austenitic steel [20,21,36,55] and ferritic steel [29].

Furthermore, the comparison of profiles of well-developed extrusions obtained by AFM with respect to the crystallographic orientation of activated slip system showed agreement with previous findings by Villechaise et al. [19,22]. The slope at one side of an extrusion observable by AFM (side A in figure 15(e)) is identical to the computed slip plane inclination. This AFM/EBSD analysis was however always limited only to this side where the emerging active slip plane is inclined to the surface at an obtuse angle. More coherent picture of the PSM morphology obtained by FIB-cross-sectioning technique clearly showed that extrusions grow over the whole width of PSBs (see figure 12). It is evident from this figure that such finding could be never obtained using AFM even with an ultra-sharp tip.

The shape and the geometry of intrusions have been studied in less detail so far. The present results obtained by AFM using plastic replica and their comparison with EBSD data showed that intrusions grow in the active slip plane direction. Villechaise [22] repeatedly demonstrated by AFM for all EIPs for which inclination measurements were possible that there is a perfect continuity of the lateral flat surface between the intrusion and extrusion part and thus suggesting that intrusions grow along the PSB/matrix interface. In agreement with our previous results obtained by high-resolution SEM-FEG [20,21,29,36,55] the thickness of intrusions were found to be much lower than extrusions (typically by a factor of 4 and less).

4.4. *Quantitative data on the growth of extrusions and intrusions*

Present experimental data on the kinetics of extrusion growth are in good agreement with the results obtained previously for several materials – mono- and polycrystalline copper [59], 316L steel [20,21], ferritic steel [21,29] and ferritic-pearlitic and alloyed ferritic-pearlitic steels [28]. In all cases the short period of rapid extrusion growth was followed by the period of stable (linear) growth (see figure 15(e)). Stable linear growth of extrusions with different growth rate in the range of 0.013–0.098 nm/cycle was found by Salazar et al. for γ-phase in austenitic-ferritic duplex stainless steel [34]. Linear growth of extrusions can be inferred from limited data also for the nickel-base superalloy Waspaloy [32].

Quantitative data on the growth of intrusions show that intrusions appear very early (see figure 11) and their depth increases linearly with the number of cycles. As it was mentioned above the rate of their growth is higher than that of extrusions and depends on the type of EIPs. The data on the intrusion growth seem to be in contradiction with those reported by Nakai et al. [12, 24] and Wang et al. [25] but as will be shown below they are consistent with both of them.

Nakai et al. studied the growth of intrusions in fine [12,24] and coarse [24] grained α-brass fatigued in cyclic plane bending with different stress amplitudes. They plotted the experimental data into a semi-logarithmic chart (i.e. intrusion depth vs. $\log N$) and found that the intrusion depth increases linearly with the logarithm of the number of cycles. In addition they identified a 'drastic' increase in the growth of intrusion depth in their semi-logarithmic presentation of experimental data which was interpreted as the outgrowth of an intrusion to a crack [12,24]. Using the identical philosophy a similar conclusion was drawn by Wang et al. from their much more thorough AFM/EBSD study of intrusion growth in 316L steel cyclically strained in torsion [25]. Re-plotting their data into linear charts (i.e. intrusion depth

vs. *N*), however, shows that the observed 'drastic' increase in growth of the intrusion depth is only virtual. Intrusions in this representation grow linearly within the scatter of experimental data [24,25].

The results obtained by Nakai et al. [24] nevertheless indicate another interesting feature concerning the true outgrowth of an intrusion to a microcrack which was not discussed by the authors. They documented the growth of an intrusion by AFM on a series of profiles from cross-sections taken at different stages in the same location on the replica (see figure 5 in [24]). It is very important to note that all replicas were taken always at the maximum tensile stress (not in unloaded state). In spite of the fact that plastic replica does not reflect truly intrusion/microcrack for $N \geq 9.1\times10^4$ it is clearly seen from their figure that there is no difference in the height of the matrix on both sides of the intrusion until $N = 4.7\times10^4$ while with further cycling a slip offset along one of its side is detectable. This finding indicates that an intrusion outgrew really into a crack via slipping-unslipping mechanism discussed in [2,8].

4.5. *Comparison of experimental data with theoretical models*

Experimental results concerning the characteristic changes of the shape of PSMs and the kinetics of extrusion and intrusion growth (see figure 15) can be reconciled with some recent models of surface relief evolution and fatigue crack initiation. Detailed comparison of the present experimental data with all the latest theoretical models and computer simulations was presented already in the part 1 [2] and thus in the following we will briefly discuss only those pertinent to the results of this study.

According to figure 15(e) the process of surface relief formation can be divided into two characteristic stages. The stage I comprising the short early period of the rapid extrusion growth is in a very good agreement with the EGM model by Essmann et al. [61] which predicts rapid initial development of a static extrusion with triangular profile. However, for the explanation of further systematic growth of extrusions and intrusions with cycling (stage II in figure 15(e)) some other mechanisms must be considered. Polák in his model [8,38,62, 63] supposes that after the formation of a static extrusion resulting from the accumulation of vacancy type point defects in the PSB, the migration of vacancies from a PSB to the matrix results in redistribution of the matter. This redistribution leads to the accumulation of atoms in the PSB and deficiency of atoms at the boundary between the PSB and the matrix. It manifests in the ongoing growth of an extrusion and the formation and growth of one or two

intrusions. It is in agreement with statistical evaluation of the intrusion occurrence (see figure 10).

4.6. *Role of PSB/matrix interface in fatigue crack initiation*

The distinguished role of the interface between PSBs and matrix as a preferential site for the initiation of fatigue cracks has been recognized and repeatedly documented experimentally by many researches. In addition, some of them have even specified explicitly the preferred sites of crack nucleation or intrusion formation within the PSMs, i.e. the sign of EIPs. Experimental results on this topic have been collected and systematized firstly by Brown and Ogin in 1985 [64]. Table 2 represents an extended and upgraded version of their table supplemented by the type of experimental technique used for surface relief observation and number of cycles when the observations were carried out. Note that except the work by Basinski and Basinski [76] (see table 2) all fatigue tests were performed at room temperature. Both individual PSMs and macro-PSMs are included in this table deliberately in order to avoid any confusion. Fatigue crack initiation in macro-PSMs, typically found only in single crystals, represents a special case due to the specific dislocation structure of macro-PSBs. It is moreover complicated by other effects (local lattice rotation, local bending of the primary slip plane) [2].

[Insert table 2 about here]

The topography and the crack initiation within individual PSMs were studied using various techniques in a wide variety of materials, both single- and polycrystalline, fatigued under diverse testing conditions to different stages of fatigue life. Considering the scheme shown in figure 9 we can see from table 2 that intrusions (or already initiated microcracks) were detected either only at the side A or B or along both sides (A/B type) or even within an individual PSM. Note that the detection of an intrusion at the side B of a well-developed PSM (see figures 3 and 15(e)) is much more delicate and that intrusions or initiated microcracks at this position can escape observation during the direct viewing of the specimen with the electron beam perpendicular to the surface (compare for example figure 8 in [43] and PSM I in figure 5 in [29]). In conclusion, the data summarized in table 2 clearly show that there is variability in observed morphology of individual PSMs and no general agreement on the preferential site of crack nucleation within individual PSMs, i.e. on the sign of EIPs. Such finding can be reconciled with the results presented in figure 10. This figure, based on the

systematic monitoring of the morphology of nearly 200 individual PSMs in differently oriented grains of 316L steel, also reveals variability in the appearance of PSMs at different early stages of their evolution. This variability has decreasing tendency with continuing cycling and after 6750 cycles (~ 15% N_f) nearly 90% of extrusions are accompanied by two parallel intrusions going simultaneously along both PSB/matrix interfaces.

Concerning the sign of the first EIPs the present results show that the first intrusions start much more frequently at the side B of the extrusion where the emerging active slip plane is inclined to the surface at an acute angle (see figure 11). This finding can be compared with several theoretical models. Essmann et al. [61] and Brown and co-workers [64] modeled only the presence of an extrusion and crack initiation either on A or B side. EGM simply proposed that sharper notch formed at B side of a static extrusion should be preferred for crack initiation. This geometrical consideration is in agreement with the numerical simulations by Repetto and Ortiz [78]. The profiles of their simulations appear to be realistic, however, the kinetics of extrusion and mainly intrusion growth are not in agreement with the experimental results. They considered individual PSB in copper single crystal fatigued with high plastic strain amplitude (6×10^{-3}). After 60,000 cycles an intrusion at the side B reached the depth only of 14 nm. Conclusions by Brown and co-workers [64] (see also [2]) with regard to the preferential side of intrusion formation are in agreement with present experimental results if macroscopic internal tensile stress is present in a PSB. However, other aspects of the model are difficult to reconcile with stable simultaneous growth of extrusions and intrusions [2]. Also the experimental fact that early in the cycling intrusions can appear only locally at the extrusion/matrix interface support more likely an idea of gradual intrusion formation due to the vacancy migration from PSB to the matrix than fatigue crack initiation by decohesion due to logarithmic infinities in stress developed at PSB/matrix interface at the crystal surface. Summarizing the above statements there are two arguments for preference of the B side for crack initiation: (i) the notch developed at B side is sharper and (ii) the largest plastic slip within a PSB results, according to the finite element calculations by Sauzay and Gilormini [79], at surface, along the PSB-matrix interface at location B.

5. Final remarks

Present work pointed out some difficulties in the surface relief study of polycrystals. Generally, there is considerable variability in the surface relief topography of PSMs. Quantitative data on the growth of extrusions and intrusions can differ from grain to grain but

a scatter in their growth characteristics can be found even within an individual grain. This is partially due to the fact that both extrusion and intrusion grow in the direction of the active Burgers vector and the height of extrusions is proportional to the grain size bellow the surface [18]. Further complication arises from the fact that there is a big scatter in local shear strain amplitudes within PSBs, even in one grain, and that the slip activity in PSBs has spatio-temporal character, as it was recently evidenced for PSBs in polycrystalline nickel [80,81]. All the above features indicate the importance of statistical approach in surface relief study in fatigued polycrystals.

6. Conclusions

Detailed AFM study of the early stages of surface relief evolution and the growth of extrusions and intrusions performed simultaneously on the specimen surface and its inverse copy obtained using plastic replicas with respect to the crystallographic orientation of individual grains in polycrystalline austenitic 316L steel cycled at room temperature with $\varepsilon_{ap} = 1\times10^{-3}$ up to 15% of the fatigue life leads to the following conclusions:

(1) Localization of the cyclic plastic strain starts very early in fatigue life and PSBs are formed. Plastic strain in majority of grains is accommodated mostly by one slip system.

(2) At the very early stage of cycling (N < 10–50 cycles) fine slip markings appear at sites where true PSMs develop later. In the great majority of grains most of these fine SMs become areas of permanent slip activity manifested by gradually growing PSMs.

(3) The appearance of the first PSMs corresponds to the onset of cyclic softening and to the characteristic changes of the loop shape parameter V_H.

(4) PSMs start as fine surface extrusions which later widen and heighten. After some delay (200–1 000 cycles) intrusions arise at the boundary with the matrix and deepen progressively.

(5) The first intrusions appear much more frequently at the side of extrusions where the emerging active slip plane is inclined to the surface at an acute angle.

(6) Already after 2 000 cycles (4.3% N_f) more than 96% of extrusions are accompanied by at least one parallel intrusion (68% by two intrusions).

(7) Typical morphology of mature PSMs developed after 6 750 cycles (15% N_f) consists of ribbon-like extrusions accompanied by two thin parallel intrusions running along PSB/matrix interfaces.

(8) The details of surface geometry of PSMs and the kinetics of systematic and simultaneous growth of extrusions and intrusions are in agreement with vacancy models of surface relief evolution in which the redistribution of matter between PSBs and matrix is considered.

Acknowledgements

Authors are indebted to Mr. J. Dymáček for his careful performing of fatigue tests, to Dr. M. Petrenec for his help with the statistical data processing and to Dr. T. Vystavěl (FEI Company in Brno) for his skilful co-operation during the preparation and documentation of FIB sections. The support of the present work by the grants No. 106/06/1096 and No. 101/07/1500 of the Grant Agency of the Czech Republic and by the research project No. AV0Z 2041057 and grant No. 1QS200410502 of the Academy of Sciences of the Czech Republic is acknowledged.

References

[1] J.A. Ewing and J.C.W. Humfrey, Phil. Trans. Roy. Soc. (London) A 200 (1903) p. 241.

[2] J. Man, K. Obrtlík and J. Polák, Phil. Mag. (2008), submitted for publication.

[3] P. Neumann, *Fatigue*, in *Physical Metallurgy*, 3rd. ed., Part 2, Chapter 24, R. W. Cahn and P. Haasen, eds., Elsevier Science, Amsterdam, 1983, pp. 1554–1594.

[4] H. Mughrabi, *Dislocations in fatigue*, in *Dislocations and Properties of Real Materials*, Book No. 323, The Institute of Metals, London, 1985, pp. 244–262.

[5] C. Laird, *Fatigue*, in *Physical Metallurgy*, R.W. Cahn and P. Haasen, eds., 4th ed., Vol. 3, Chapter 27, Elsevier Science, Amsterdam, 1996, pp. 2293–2397.

[6] S. Suresh, *Fatigue of Materials*, 2nd ed., Cambridge University Press, Cambridge, 1998.

[7] P. Lukáš, *Fatigue crack initiation mechanisms*, in *Encyclopedia of Materials: Science and Technology*, Vol. 3, K.H.J. Buschow, R.W. Cahn, M.C. Flemings et al., eds., Elsevier Science, Oxford, 2001, pp. 2884–2894.

[8] J. Polák, *Cyclic deformation, crack initiation, and low-cycle fatigue*, in *Comprehensive Structural Integrity*, Vol. 4, I. Milne, R.O. Ritchie and B. Karihallo, eds., Elsevier, Amsterdam, 2003, pp. 1–39.

[9] P. Lukáš and L. Kunz, Phil. Mag. 84 (2004) p. 317.

[10] S.E. Harvey, P.G. Marsh and W.W. Gerberich, Acta metall. mater. 42 (1994) p. 3493.

[11] Y. Nakai, S. Fukuhara and K. Ohnishi, Int. J. Fatigue 19 (1997) p. S223.

[12] Y. Nakai, K. Ohnishi and T. Kusukawa, *Observations of fatigue slip bands and stage I crack-initiation process in α-brass using scanning atomic-force microscopy*, in *Small Fatigue Cracks: Mechanics, Mechanisms and Applications*, K.S. Ravichandran, R.O. Ritchie, and Y. Murakami, eds., Elsevier Science Ltd., Oxford, 1999, pp. 343–352.

[13] J. Polák, J. Man and K. Obrtlík, *Observation of fatigue damage in crystalline materials using atomic force microscopy*, in *Advances in Mechanical Behaviour, Plasticity and Damage*, *Proceedings of EUROMAT 2000*, Vol. 2, D. Miannay, P. Costa, D. François and A. Pineau, eds., Elsevier, Oxford, 2000, pp. 1161–1166.

[14] L. Cretegny and A. Saxena, Acta Mater. 49 (2001) p. 3755.

[15] M.R. Stoudt, R.E. Ricker and R.C. Cammarata, Int. J. Fatigue 23 (2001) p. S215.

[16] J. Ma, Mater. Sci. Eng. A 457 (2007) p. 63.

[17] S. Stanzl-Tschegg, H. Mughrabi and B. Schoenbauer, Int. J. Fatigue 29 (2007) p. 2050.

[18] J. Man, K. Obrtlík, C. Blochwitz et al., Acta Mater. 50 (2002) p. 3767.

[19] P. Villechaise, L. Sabatier and J.C. Girard, Mater. Sci. Eng. A 323 (2002) p. 377.

[20] J. Man, K. Obrtlík and J. Polák, Mater. Sci. Eng. A 351 (2003) p. 123.

[21] J. Polák, J. Man and K. Obrtlík, Int. J. Fatigue 25 (2003) p. 1027.

[22] P. Villechaise, *Combination of electron back scattering diffraction and atomic force microscopy investigations for the study of slip bands induced by fatigue in a stainless steel*, in *ATEM '03*, *Proceedings of International Conference on Advanced Technology in Experimental Mechanics 2003*, JSME No. 03-207, The Japan Society of Mechanical Engineers (JSME-MMD), Tokyo, 2003, CD ROM, paper No. OS05W0392.

[23] J. Wejdemann and O.B. Pedersen, Mater. Sci. Eng. A 387–389 (2004) p. 556.

[24] Y. Nakai, T. Kusukawa and N. Hayashi, *Scanning atomic-force microscopy on initiation and growth behavior of fatigue slip-bands in α-brass*, in *Fatigue and Fracture Mechanics: 32nd Volume*, ASTM STP 1406, R. Chona, ed., American Society for Testing and Materials, West Conshohocken, PA, 2001, pp. 122–135.

[25] Y. Wang, H. Kimura, Y. Akiniwa et al., Key Eng. Mater. 340–341 (2007) p. 531.

[26] T. Yamasaki, Y. Kaneko, H. Miyamoto et al., Mater. Sci. Eng. A 319–321 (2001) p. 569.

[27] L. Cretegny and A. Saxena, Fatigue Fract. Engng. Mater. Struct. 25 (2002) p. 305.

[28] E. Abe, T. Tagawa and T. Miyata, *AFM observation of evolution of slip deformation by high cycle fatigue in low carbon steels*, in *ATEM '03*, *Proceedings of International Conference on Advanced Technology in Experimental Mechanics 2003*, JSME No. 03-207, The Japan Society of Mechanical Engineers (JSME-MMD), Tokyo, 2003, CD ROM, paper No. OS05W0273.

[29] J. Man, M. Petrenec, K. Obrtlík et al., Acta Mater. 52 (2004) p. 5551.

[30] B. Fournier, M. Sauzay, C. Caës et al., Int. J. Fatigue 30 (2008) 1797.

[31] K. Obrtlík, J. Man, M. Petrenec et al., *Cyclic strain localization in Inconel 713 LC at room and high temperature*, in *FATIGUE 2002*, *Proceedings of the Eight International Fatigue Congress*, Vol. 2/5, A.F. Blom, ed., EMAS, West Midlands, UK, 2002, pp. 963–970.

[32] M. Risbet, X. Feaugas, C. Guillemer-Neel et al., Scripta Mater. 49 (2003) p. 533.

[33] M. Risbet, X. Feaugas, C. Guillemer-Neel et al., Scripta Mater. 60 (2009) p. 269.

[34] D. Salazar, I. Serre and J.-B. Vogt, *Using atomic force microscopy to study cyclic plasticity mechanisms in a DSS-25Cr-7Ni-0.25N*, in *DUPLEX 2007, Proceedings of the 7th International Conference & Expo*, CD-ROM, Associazione Italiana di Metallurgia, Milano, 2007.

[35] D. Salazar, I. Serre and J.-B. Vogt, *LCF mechanisms of the 25Cr-7Ni-0.25N duplex stainless steel investigated by atomic force microscopy*, in *Sixth International Conference on*

Low Cycle Fatigue (LCF 6), P.D. Portela, T. Beck and M. Okazaki, eds., DVM, Berlin, 2008, pp. 85–90.

[36] J. Polák, J. Man, K. Obrtlík et al., Z. Metallkd. 94 (2003) p. 1327.

[37] J. Polák, J. Man and K. Obrtlík, Mater. Sci. Forum 482 (2005) p. 45.

[38] J. Polák, Mater. Sci. Eng. A 468–470 (2007) p. 33.

[39] J. Polák, J. Helešic and K. Obrtlík, Mater. Sci. Eng. A 101 (1988) p. 7.

[40] J. Polák, J. Man, T. Vystavěl et al., Key Eng. Mater. 345-346 (2007) p. 379.

[41] S. Ortner, C. Laird and G.C. Farrington, Acta metal. 35 (1987) p. 453.

[42] A. Hunsche and P. Neumann, *On the formation of extrusion-intrusion pairs during fatigue of copper*, in *Advances in Fracture Research*, *Proceedings of the 5th International Conference on Fracture (ICF 5)*, Vol. 1, D. François, ed., Pergamon Press, Oxford, 1981, pp. 273–279.

[43] H. Mughrabi, R. Wang, K. Differt et al., *Fatigue crack initiation by cyclic slip irreversibilities in high-cycle fatigue*, in *Fatigue Mechanisms: Advances in Quantitative Measurement of Physical Damage*, ASTM STP 811, J. Lankford, D.L. Davidson, W.L. Morris and R.P. Wei, eds., American Society for Testing and Materials, Philadelphia, 1983, pp. 5–45.

[44] Z.S. Basinski and S.J. Basinski, Scripta metall. 18 (1984) p. 851.

[45] B.-T. Ma and C. Laird, Acta metall. 37 (1989) p. 325.

[46] Z.S. Basinski and S.J. Basinski, Prog. Mater. Sci. 36 (1992) p. 89.

[47] C. Blochwitz, J. Brechbühl and W. Tirschler, Mater. Sci. Eng. A 210 (1996) p. 42.

[48] M. Sauzay and T. Jourdan, Int. J. Fracture 141 (2006) p. 431.

[49] M. Sauzay, Acta Mater. 55 (2007) p. 1193.

[50] M. Sauzay and J. Man, Mater. Sci. Forum 567-568 (2008) p. 149.

[51] H. Mughrabi, Mater. Sci. Eng. 33 (1978) p. 207.

[52] Y. Kaneko, Y. Morita and S. Hashimoto, Scripta Mater. 37 (1997) p. 963.

[53] J. Man, A. Weidner, K. Obrtlík et al., to be published.

[54] A. Hunsche and P. Neumann, Acta metall. 34 (1986) p. 207.

[55] J. Polák and T. Kruml, *Topography of the crack nuclei at the emerging persistent slip band in austenitic 316L steel*, in *Low Cycle Fatigue and Elasto-Plastic Behaviour of Materials*, K.-T. Rie and P.D. Portella, eds., Elsevier Science, Oxford, 1998, pp. 559–564.

[56] I.B. Kwon, M.E. Fine and J. Weertman, Acta metal. 37 (1989) p. 2927.

[57] G.-H. Kim, I.-B. Kwon and M.E. Fine, Mater. Sci. Eng. A 142 (1991) p. 177.

[58] R. Wang, B. Bauer and H. Mughrabi, Z. Metallkd. 73 (1982) p. 30.

[59] H. Mughrabi, M. Bayerlein and R. Wang, *Direct measurement of the rate of extrusion growth in fatigued copper mono- and polycrystals*, in *Proceedings of the Ninth International Conference on Strength of Metals and Alloys (ICSMA 9)*, Vol. 2, D.G. Brandon, R. Chaim and A. Rosen, eds., Freund Publ. Comp., London, 1991, pp. 879–886.

[60] K. Differt, U. Essmann and H. Mughrabi, Phil. Mag. A 54 (1986) p. 237.

[61] U. Essmann, U. Gösele and H. Mughrabi, Phil. Mag. A 44 (1981) p. 405.

[62] J. Polák, Mater. Sci. Eng. 92 (1987) p. 71.

[63] J. Polák and M. Sauzay, Mater. Sci. Eng. A 500 (2009) p. 122.

[64] L.M. Brown and S.L. Ogin, *Role of internal stresses in the nucleation of fatigue cracks*, in *Fundamentals of Deformation and Fracture*, B.A. Bilby, K.J. Miller and J.R. Willis, eds., Cambridge University Press, Cambridge, 1985, pp. 501–528.

[65] M. Hempel, *Metallographic observations on the fatigue of steels*, in *Proceedings of the International Conference on Fatigue of Metals*, The Institution of Mechanical Engineers, London, 1956, pp. 543–547.

[66] A.W. Wood, *Some basic studies of fatigue in metals*, in *Fracture*, B.L. Averbach, D.K. Felbeck, G.T. Hahn and D.A. Thomas, eds., The Technology Press of Massachusetts Institute of Technology and John Wiley & Sons, New York, 1959, pp. 412–434.

[67] R.C. Boettner and A.J. McEvily, Acta Metall. 13 (1965) p. 937.

[68] E.E. Laufer and W.N. Roberts, Phil. Mag. 14 (1966) p. 65.

[69] P. Neumann, Z. Metallk. 58 (1967) p. 780.

[70] P. Lukáš and M. Klesnil, Phys. Stat. Sol. 37 (1970) p. 833.

[71] J. Dönch and P. Haasen, Z. Metallk. 62 (1971) p. 780.

[72] K. Katagiri, A. Omura, K. Koyanagi, et al., Met. Trans. 8A (1977) p. 1769.

[73] H.N. Hahn and D.J. Duquette, Acta Metall. 26 (1978) p. 279.

[74] J. Polák, T. Lepistö and P. Kettunen, Mater. Sci. Eng. 74 (1985) p. 85.

[75] A. Hunsche and P. Neumann, Acta metall. 34 (1986) p. 207.

[76] Z.S. Basinski and S.J. Basinski, Acta metall. 37 (1989) p. 3263.

[77] J.I. Dickson, J.-P. Baïlon, J. Xia et al., *Extrusion-intrusion formation in Cu and 70Cu-30Zn*, in *Proceedings of the Fifth International Conference on Fatigue and Fatigue Thresholds (FATIGUE `93)*, Vol. III, J.-P. Baïlon and J.I. Dickson, eds., EMAS, West Midlands, UK, 1993, pp. 1883–1892.

[78] E.A. Repetto and M. Ortiz, Acta mater. 45 (1997) p. 2577.

[79] M. Sauzay and P. Gilormini, Theor. Appl. Fract. Mech. 38 (2002) p. 53.

[80] A. Weidner, R. Beyer, C. Blochwitz et al., Mater. Sci. Eng. A 435–436 (2006) p. 540.

[81] A. Weidner, J. Man, W. Tirschler et al., Mater. Sci. Eng. A 492 (2008) p. 118.

Figure captions

Figure 1. Cyclic hardening/softening curve of 316L steel cycled with constant $\varepsilon_{ap}=1\times10^{-3}$ with indicated sequences of AFM surface relief inspection by direct observation of metallic specimen and via plastic replica.

Figure 2. Inverse pole figure as obtained by the analysis of EBSD measurement for 32 surface grains in 316L steel. Slip activities in individual grains correspond to N = 500 cycles and more (cf. figure 4).

Figure 3. Schematic drawing of four possibilities of slip plane inclination relative to the specimen surface (i.e. x_s–y_s plane in the specimen co-ordinate system x_s–y_s–z_s). The angles φ and β_1 are the angles between the stress axis and the intersection of the active slip plane with the specimen surface and the plane perpendicular to the specimen surface and parallel to the stress axis, respectively.

Figure 4. Frequency of grains with different slip activities within 32 surface grains of 316L steel cycled with $\varepsilon_{ap} = 1\times10^{-3}$ (P and S denote primary and secondary slip system (ss), respectively).

Figure 5. Early stages of surface relief evolution within the grain No. 62 of 316L steel cycled with $\varepsilon_{ap} = 1\times10^{-3}$ as obtained by AFM observation of specimen surface. (a) N = 10 cycles (0.02% N_f), (b) N = 50 cycles (0.1% N_f), (c) N = 100 cycles (0.2% N_f), (d) N = 200 cycles (0.4% N_f), (e) N = 1000 cycles (2.2% N_f), (f) N = 3000 cycles (6.5% N_f). The scale of all micrographs is identical. The AFM images are displayed in the shadowed format. Wavy features running horizontally across some micrographs (visible particularly in figure 5(b) and 5(d)) are parallel with the scanning direction and they represent AFM feedback artefacts which do not reflect defect structure or slip topography.

Figure 6. Early stages of surface relief evolution within the grain No. 78 of 316L steel cycled with $\varepsilon_{ap} = 1\times10^{-3}$ as obtained by AFM using plastic replicas. (a) N = 350 cycles (0.8% N_f), (b) N = 500 cycles (1.1% N_f), (c) N = 750 cycles (1.6% N_f), (d) N = 2000 cycles (4.3% N_f). The three-dimensional AFM micrographs of plastic replicas are displayed in non-inverted format.

Figure 7. Development of surface relief profiles in the cross-section A marked in figure 5(e) as detected by AFM on the metallic specimen within the grain No. 62 of 316L steel cycled

with $\varepsilon_{ap} = 1\times10^{-3}$. Profiles in the early and later stages are shown in the scale one-to-six (a) and one-to-one (b), respectively. The positions of fine SMs 7, 9 and 10 that appeared after 10 cycles are indicated by the vertical dashed lines; β is the angle of inclination of active slip plane to the specimen surface as calculated from EBSD measurements (see table 2).

Figure 8. Number of grains with given persistency of localized cyclic slip, p_s, in specimen of 316L steel cycled with $\varepsilon_{ap} = 1\times10^{-3}$.

Figure 9. Typical configurations of extrusion-intrusion pairs observed in fatigued 316L.

Figure 10. Evolution of morphology of 197 PSMs in 31 surface grains of 316L steel cycled with constant $\varepsilon_{ap}=1\times10^{-3}$.

Figure 11. Occurrence of individual PSMs in 31 surface grains of 316L steel at the moment when the first intrusions appear.

Figure 12. SEM-FEG micrograph of a cross-sectioned individual PSM in 316L cycled with $\varepsilon_{ap} = 1\times10^{-3}$. PSM was sectioned by FIB after 500 cycles and then fatigued to 2000 cycles.

Figure 13. Simultaneous growth of extrusions and intrusions in the grains of 316L steel at the beginning of cycling with $\varepsilon_{ap} = 1\times10^{-3}$. (a) the grain No. 59 – extrusion and one parallel intrusion, (b) the grain No. 52 – extrusion and two parallel intrusions.

Figure 14. Correlation between the onset of PSM appearance, cyclic hardening/softening curve and the hysteresis loop changes characterized by the loop shape parameter V_H in 316L steel fatigued with constant plastic strain amplitude. SM – slip marking, PSM – persistent slip marking.

Figure 15. Schematic illustration of the consecutive characteristic stages of surface relief evolution in 316L steel fatigued with constant plastic strain amplitude of 1×10^{-3} at room temperature. (a) Fine SMs with tensile (and/or compressive) slip steps, (b) true PSMs with ribbon-like "static" extrusions, (c) growing extrusions and intrusions starting at PSB/matrix interfaces, (d) mature PSMs with well developed ribbon-like extrusions accompanied by two parallel intrusions at both PSB/matrix interfaces, (e) the kinetics of the growth of extrusions and intrusions.

Table 1. Slip systems and their crystallographic characteristics as obtained by EBSD within 32 surface grains of fatigued 316L steel.

Grain	Stress axis†	Slip systems‡			Schmid factor μ	Orientation factor Q§	Angle of inclination of PSM to the stress axis φ		Angle β_1¶	Angle of slip plane to the surface β	Angle of slip direction to the surface α
							Observed	Calculated			
50	[51 $\overline{49}$ 20]	P	(111)[$\bar{1}$01]	III	0.429	0.972	–55.2°	–55.9°	44.0°	49.4°	46.4°
51	[$\overline{99}$ 52 48]	P	(111)[$\bar{1}$01]	I	0.418	0.945	42.3°	42.3°	35.4°	46.6°	14.6°
52	[$\overline{72}$ $\overline{57}$ $\overline{94}$]	P	(111)[$\bar{1}$01]	IV	0.389	0.853	–57.5°	–55.1°	–30.5°	35.7°	15.4°
		S_2	($\bar{1}\,\bar{1}$1) [011]	I	0.310		22.5°	21.0°	55.0°	75.9°	22.4°
53	[$\bar{1}$ 99 $\overline{35}$]	S_1	($\bar{1}$11)[101]	III	0.490	0.996	–64.4°	–65.3°	52.0°	54.7°	32.7°
54	[$\overline{83}$ $\overline{29}$ 11]	P	(111)[$\bar{1}$01]	III	0.494	0.931	–76.8°	–75.4°	41.9°	42.8°	41.1°
55	[48 59 $\overline{57}$]	P	(111)[$\bar{1}$01]	I	0.329	0.979	40.8°	42.4°	27.6°	37.8°	4.1°
56	[$\overline{57}$ $\overline{90}$ 31]	P	(111)[$\bar{1}$01]	I	0.465	0.748	85.4°	84.3°	37.2°	37.3°	34.3°
57	[$\overline{20}$ 77 $\overline{51}$]	P	(111)[$\bar{1}$01]	I	0.479	0.806	45.1°	46.0°	58.7°	66.4°	33.8°
58	[$\overline{39}$ $\overline{61}$ 88]	P	(111)[$\bar{1}$01]	I	0.440	0.786	53.4°	53.6°	37.8°	43.9°	17.6°
59	[$\overline{42}$ $\overline{94}$ 23]	P	(111)[$\bar{1}$01]	III	0.485	0.854	–87.0°	–86.1°	38.2°	38.3°	38.2°
		S_2	($\bar{1}\,\bar{1}$1) [$\bar{1}$01]	IV	0.375		–44.0°	–40.5°	–28.0°	39.3°	19.6°
60	[46 99 $\overline{32}$]	P	(111)[$\bar{1}$01]	II	0.467	0.833	83.2°	79.6°	–35.2°	35.7°	33.5°
61	[$\overline{93}$ $\overline{35}$ 27]	P	(111)[$\bar{1}$01]	I	0.466	0.899	79.8°	81.2°	34.6°	34.9°	34.3°
62	[9 51 $\overline{86}$]	P	(111)[$\bar{1}$01]	I	0.492	0.925	59.8°	59.4°	54.8°	58.8°	40.8°
63	[61 $\overline{65}$ $\overline{24}$]	P	(111)[$\bar{1}$01]	II	0.435	0.956	55.7°	56.7°	–44.7°	49.8°	46.6°
64	[$\overline{12}$ 95 $\overline{58}$]	P	(111)[$\bar{1}$01]	IV	0.491	0.908	–68.4°	–68.5°	–49.3°	51.4°	46.4°
		S_1	($\bar{1}$11)[101]	I	0.446		61.2°	61.4°	73.9°	75.8°	19.9°
65	[$\overline{93}$ 9 47]	P	(111)[$\bar{1}$01]	III	0.499	0.936	–45.5°	–46.8°	80.4°	82.9°	4.3°
		S_1	($\bar{1}$11)[101]	II	0.467		69.8°	70.2°	–59.4°	60.9°	42.2°
66	[27 $\overline{85}$ 40]	P	(111)[$\bar{1}$01]	II	0.469	0.821	35.3°	35.5°	–82.0°	85.4°	9.7°
		S_1	($\bar{1}\,\bar{1}$1) [011]	III	0.385		–33.7°	–33.1°	34.1°	51.1°	15.4°
67	[6 $\overline{66}$ 67]	P	(111) [$\bar{1}$01]	I	0.426	0.986	56.3°	56.3°	65.5°	69.2°	51.9°

68	[$\overline{87}$ $\overline{38}$ 87]	P	(111)[$\overline{1}$01]	III	0.419	0.998	–45.8°	–44.9°	50.5°	59.8°	46.1°
69	[55 92 $\overline{72}$]	P	(111)[$\overline{1}$01]	III	0.392	0.865	–41.7°	–42.6°	35.1°	46.1°	36.3°
70	[$\overline{49}$ $\overline{75}$ 54]	P	(111)[$\overline{1}$01]	IV	0.370	0.908	–27.0°	–26.8°	–66.7°	79.0°	25.9°
		S_1	($\overline{1}$ $\overline{1}$1) [011]	I	0.336		45.6°	44.4°	24.8°	33.5°	11.0°
71	[$\overline{85}$ 21 46]	P	(111)[$\overline{1}$01]	IV	0.486	0.833	–39.1°	–40.0°	–83.8°	86.0°	12.0°
72	[12 $\overline{3}$ $\overline{4}$]	P	(111)[$\overline{1}$01]	IV	0.471	0.902	–34.6°	–35.6°	–77.6°	82.7°	7.5°
		S_2	($\overline{1}$11) [101]	I	0.414		82.4°	82.7°	58.0°	58.2°	42.1°
73#	[56 $\overline{69}$ 23]	P	(111)[$\overline{1}$01]	III	0.455	0.857		–50.5°	49.2°	56.3°	9.6°
74	[$\overline{91}$ $\overline{44}$ 15]	P	(111)[$\overline{1}$01]	III	0.497	0.897	–67.9°	–68.7°	44.8°	46.8°	37.5°
75	[98 $\overline{7}$ $\overline{12}$]	P	(111)[$\overline{1}$01]	II	0.451	0.984	–40.8°	–40.2°	58.6°	68.5°	2.8°
		S_2	($\overline{1}$ $\overline{1}$1) [011]	III	0.426		39.2°	39.5°	–46.1°	58.6°	36.3°
76	[$\overline{81}$ $\overline{67}$ 44]	P	(111)[$\overline{1}$01]	II	0.408	0.890	–84.4°	–84.0°	31.8°	32.0°	26.9°
77	[$\overline{89}$ 65 $\overline{5}$]	P	(111)[$\overline{1}$01]	IV	0.470	0.953	–77.1°	–76.5°	–52.6°	53.4°	52.9°
		S_1	($\overline{1}$11) [101]	I	0.448		62.2°	65.9°	63.6°	65.6°	26.0°
78	[17 $\overline{11}$ 0]	P	(111)[$\overline{1}$01]	I	0.474	1.000	80.8°	80.3°	53.7°	54.1°	46.8°
		S_1	($\overline{1}$11) [101]	II	0.474		74.0°	75.6°	–54.7°	55.5°	43.1°
79	[$\overline{1}$ 70 $\overline{26}$]	P	(111)[$\overline{1}$01]	II	0.494	0.992	45.0°	47.8°	–80.0°	82.6°	15.8°
		S_1	($\overline{1}$11) [101]	III	0.490		–76.0°	–74.7°	50.1°	51.1°	41.0°
80	[20 90 $\overline{59}$]	P	(111)[$\overline{1}$01]	III	0.484	0.835	–53.1°	–52.5°	53.1°	59.2°	39.5°
81	[41 71 $\overline{37}$]	S_1	($\overline{1}$ $\overline{1}$1) [011]	III	0.379	0.927	–34.0°	–34.2°	33.7°	49.9°	27.0°

† Miller indices of stress axis in surface grains taken from **g**-matrices measured by EBSD were after all computations rounded off to double-figure for reasons of clarity (accuracy is higher than 0.1°).

‡ Primary (P) and secondary (S) slip systems identified after the transformation of Miller indices of stress axis into the standard stereographic triangle. S_1 and S_2 denote secondary slip systems with the second and the third highest Schmid factors, respectively. Roman numerals denote slip plane inclination relative to the specimen surface in agreement with the schematic drawing of a surface grain in figure 3.

§ Orientation factor $Q = \mu_{s1} / \mu_p$ where μ_{s1} and μ_p are Schmid factors of the secondary and the primary slip systems [41].

¶ Angle β_1 is the angle between the stress axis and the intersection of active slip plane with the side face (see figure 3).

No visible PSMs were detected in the grain 73 after N=6 750 cycles.

Table 2. The preferential site of crack initiation and/or intrusions in individual and macro-PSMs.

Reference	Material	Type of cycling and number of cycles	Microscopic technique†	Crack initiation (intrusion) site	Side A or side B‡
Hempel (1956) [65]	plain carbon steel (0.09% C, 0.01% Si, 0.62% Mn)	reversed plane-bending $N = 250{,}000$	TEM, plastic replica taken from longitudinal section after electroplating	at interface*	B*
Wood (1959) [66]	polycrystalline Cu	alternating torsion $N = 0.1N_f$	OM, taper-sectioning technique	at interface*	A/B*
Boettner and McEvily (1965) [67]	Fe-Si alloy single crystals	cantilever beam; fully reversed bending N not specified	OM, taper-sectioning technique	at interface	B
Laufer and Roberts (1966) [68]	Cu single crystals	plane bending $N = 20{,}000$ (~$0.01N_f$)	OM, taper-sectioning technique	at interface and quasi-periodic alternations of intrusions and extrusions along individual PSM	B
Neumann (1967) [69]	Cu single crystals	push-pull; load control $N = 200{,}000$	OM, interferometry	at interface§	A§
Lukáš and Klesnil (1970) [70]	Cu–Zn alloy single crystals	push-pull; load control $N = 0.5N_f$	TEM, surface foils after electroplating	at interface*	B*#
Dönch and Haasen (1971) [71]	Cu single crystals	push-pull; load control $N > 300{,}000$	OM, interferometry	at interface§	B§
Katagiri et al. (1977) [72]	polycrystalline Cu	plane bending; load control $N \approx 800{,}000$ ($0.8N_f$)	TEM, surface foils after electroplating	at interface*	A or B*#
Hahn and Duquette (1978) [73]	Cu single crystals	push-pull; load control $N = 100{,}000$ (~$0.07N_f$)	OM, longitudinal section after electroplating	at interface	A
Hunsche and Neumann (1981) [42]	Cu single crystals	push-pull; load control $N \approx 300{,}000$	SEM, direct observation of specimen surface	at interface	A
Mughrabi et al. (1983) [43]	Cu single crystals	push-pull; constant plastic strain $N = 1000$ or 134,000	SEM, direct observation of specimen surface	at interface	A
Basinski and Basinski (1984) [44]	Cu single crystals	push-pull; constant plastic strain $N = 5000$ and more	SEM, sharp-corner polishing technique	at interface§ and everywhere within macro-PSM	both§
Polák et al. (1985) [74]	Cu single crystals	push-pull; constant plastic strain increasing at three levels; total $N = 43{,}000$	SEM, direct observation of specimen surface	individual PSMs: at interface and quasi-periodic alternations of intrusions and extrusions within PSM macro-PSM: at interface and within macro-PSM§	A or A/B both§

Hunsche and Neumann (1986) [75]	Cu single crystals	push-pull; stress control during cyclic hardening followed by plastic strain control; $N = 30{,}000$ ($0.25N_f$) and 60,000 ($0.5N_f$)	SEM, section micromilling technique	at interface§	both§; early close to A, later longer cracks observed close to B
Ma and Laird (1989) [45]	Cu single crystals	push-pull; constant plastic strain $N = 30{,}000$ and more	SEM, sharp-corner polishing technique	at interface§	both§; longer cracks preferentially at B
Basinski and Basinski (1989) [76]	Cu single crystals	push-pull; constant plastic strain; various N for different temperatures	SEM, sharp-corner polishing technique	at interface§¶	B§
Dickson et al. (1993) [77]	polycrystalline Cu and α-brass	push-pull; constant plastic strain N not specified	SEM, direct observation of specimen surface	at interface	A (more often) or B or A/B
Polák and Kruml (1998) [55] (see also [8])	polycrystalline 316L steel	push-pull; constant plastic strain $N \approx 0.2N_f$	SEM-FEG, S and its tilting	at interface and quasi-periodic alternations of intrusions and extrusions along individual PSM	A/B
Polák et al. (2003) [21,36]	polycrystalline 316L steel	push-pull; constant plastic strain $N = 20{,}000 = N_f$	AFM and SEM-FEG, S + R and their tilting in the SEM-FEG	at interface	A/B or B (deeper intrusions always at B)
Man et al. (2004) [29]	polycrystalline ferritic steel	push-pull; constant plastic strain $N = 9{,}000 = N_f$	AFM, S + R SEM-FEG, S and its tilting	at interface and quasi-periodic alternations of intrusions and extrusions along individual PSM	A/B or B

†TEM = transmission electron microscopy, OM = optical microscopy, SEM = scanning electron microscopy, SEM-FEG = high resolution SEM equipped with field emission gun, AFM = atomic force microscopy, S = specimen surface, R = plastic replica. For details and references to some specific experimental techniques see table 1 in [2].
‡Typical morphologies of individual PSMs (in some cases already containing also initiated cracks) are denoted according to division in figure 8.
*Deduced from published micrographs.
§Interface between macro-PSMs (i.e. protrusions) and surrounding undeformed matrix. The marking of sides of macro-PSMs A or B is identical as in the case of individual PSMs (c.f. figure 2 in [2] and figure 8).
¶For fatigue at temperatures about from 15 K to 250 K in which type II PSB profiles form according to the Basinskis.
Only intrusion without any extrusion is apparent at the intersection of PSB with the specimen surface.

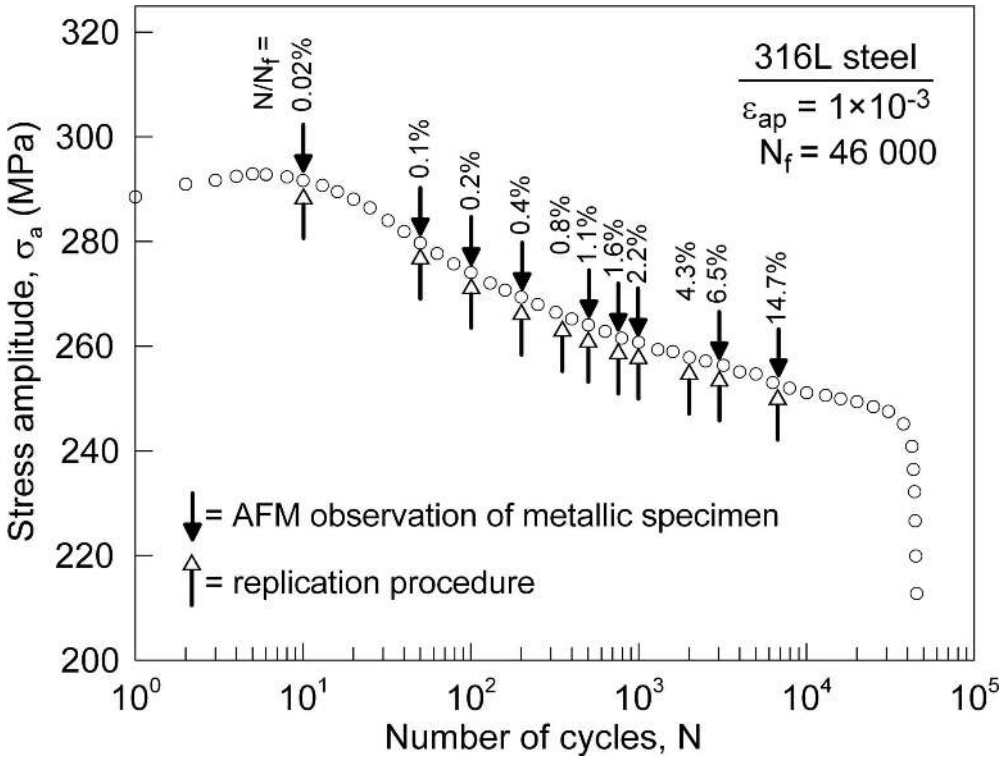

Figure 1. Cyclic hardening/softening curve of 316L steel cycled with constant ε_{ap}=1x10^{-3} with indicated sequences of AFM surface relief inspection by direct observation of metallic specimen and via plastic replica.
75x56mm (600 x 600 DPI)

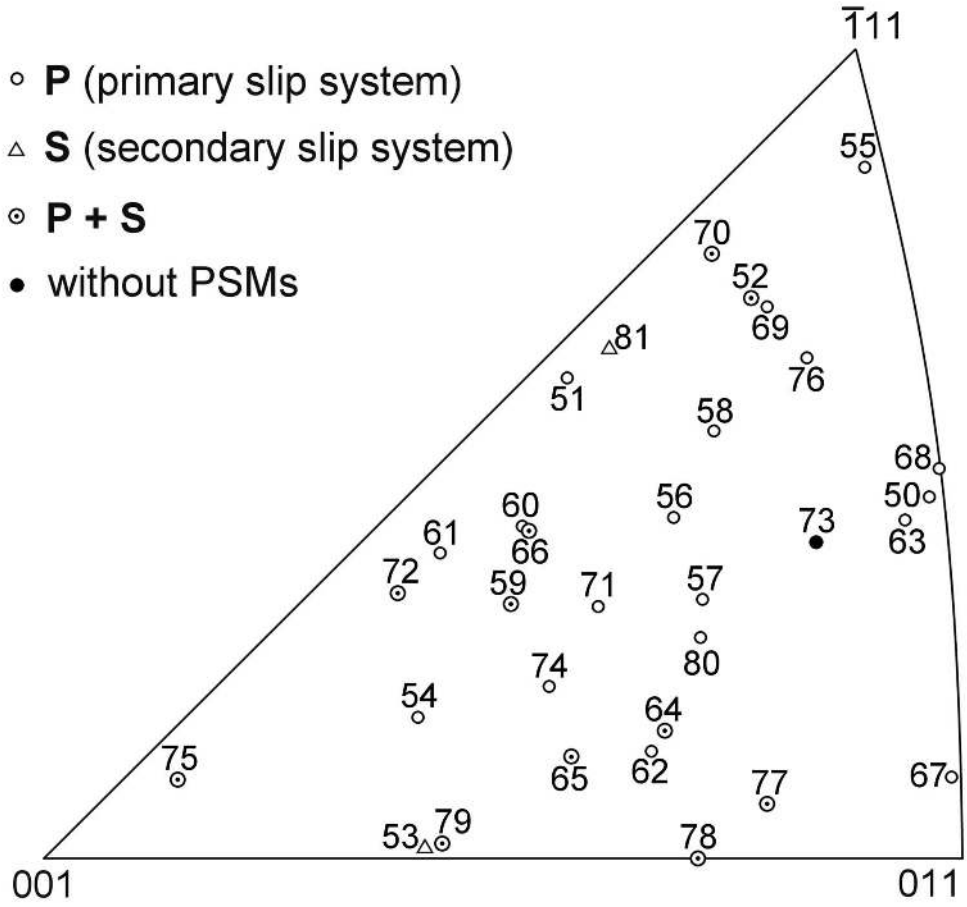

Figure 2. Inverse pole figure as obtained by the analysis of EBSD measurement for 32 surface grains in 316L steel. Slip activities in individual grains correspond to N = 500 cycles and more (cf. figure 4).
74x68mm (600 x 600 DPI)

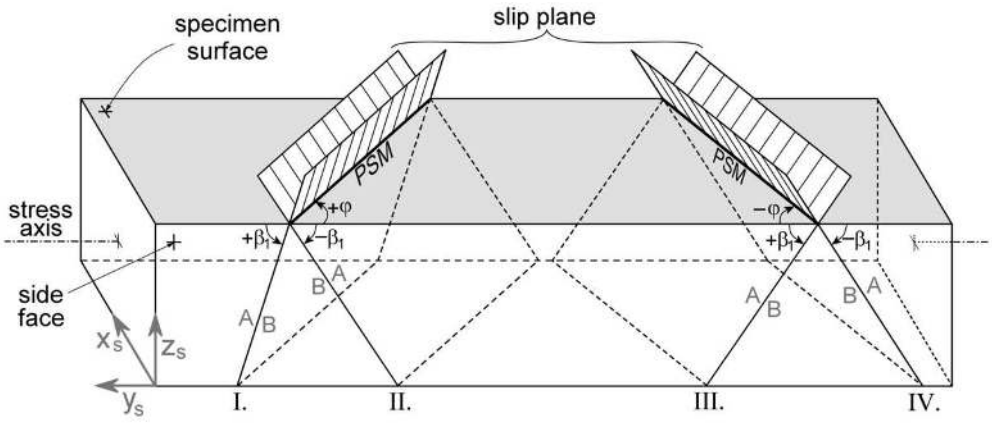

Schematic drawing of four possibilities of slip plane inclination relative to the specimen surface (i.e. x_s-y_s plane in the specimen co-ordinate system x_s-y_s-z_s). The angles φ and β_1 are the angles between the stress axis and the intersection of active slip plane with the specimen surface and the plane perpendicular to the specimen surface and parallel to the stress axis, respectively.
51x21mm (600 x 600 DPI)

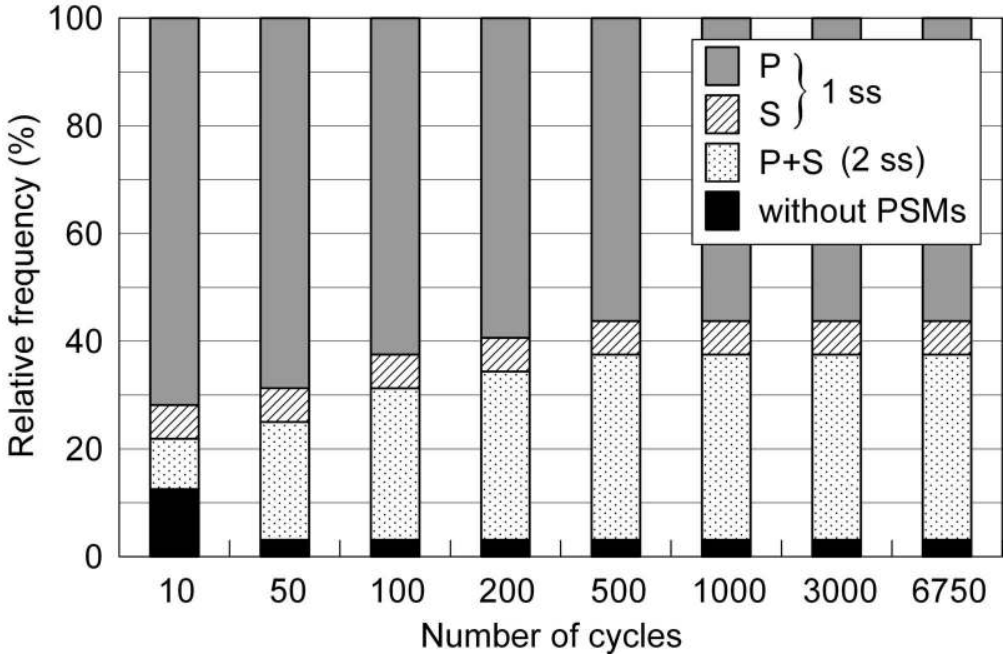

Figure 4. Frequency of grains with different slip activities within 32 surface grains of 316L steel cycled with $\varepsilon_{ap}=1x10^{-3}$ (P and S denote primary and secondary slip system (ss), respectively). 67x44mm (600 x 600 DPI)

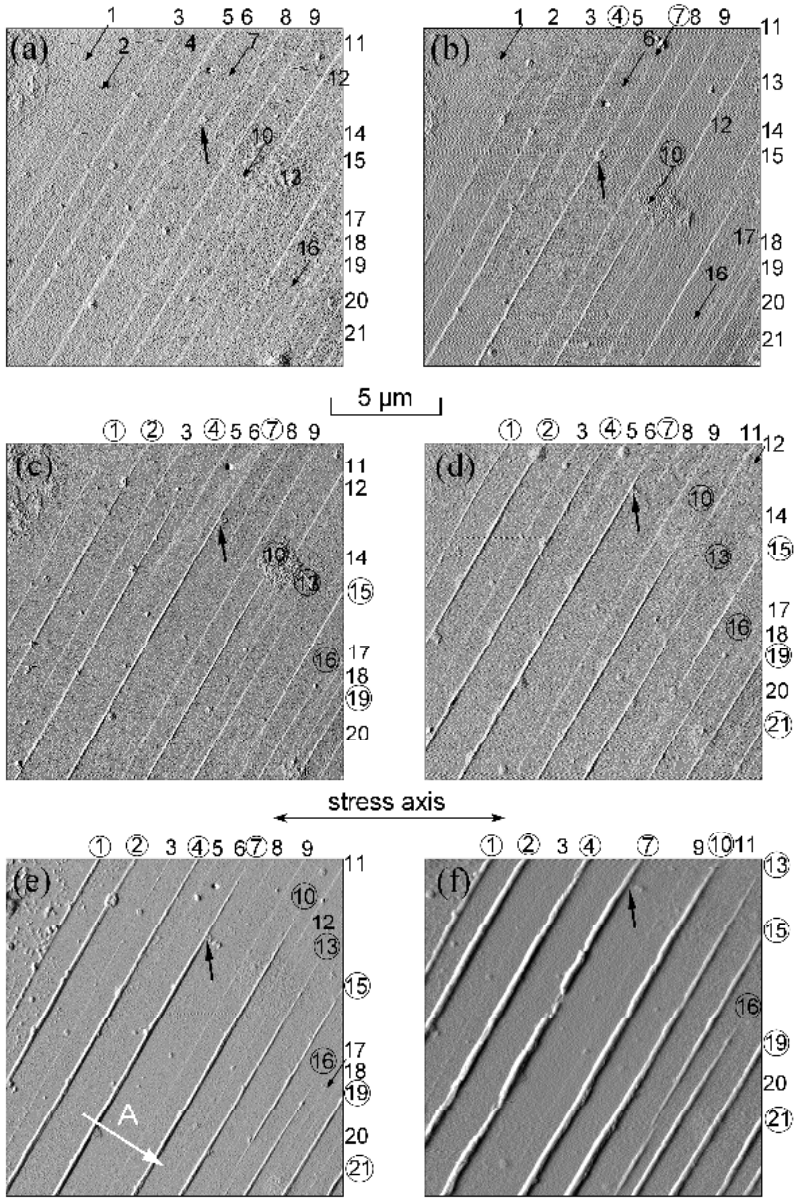

Figure 5. Early stages of surface relief evolution within the grain No. 62 of 316L steel cycled with ε_{ap}=1x10^{-3} as obtained by AFM observation of specimen surface. (a) N = 10 cycles (0.02% N_f), (b) N = 50 cycles (0.1% N_f), (c) N = 100 cycles (0.2% N_f), (d) N = 200 cycles (0.4% N_f), (e) N = 1000 cycles (2.2% N_f), (f) N = 3000 cycles (6.5% N_f). The scale of all micrographs is identical. The AFM images are displayed in the shadowed format. Wavy features running horizontally across some micrographs (visible particularly in figure 5(b) and 5 (d)) are parallel with the scanning direction and they represent AFM feedback artefacts which do not reflect defect structure or slip topography.
125x188mm (600 x 600 DPI)

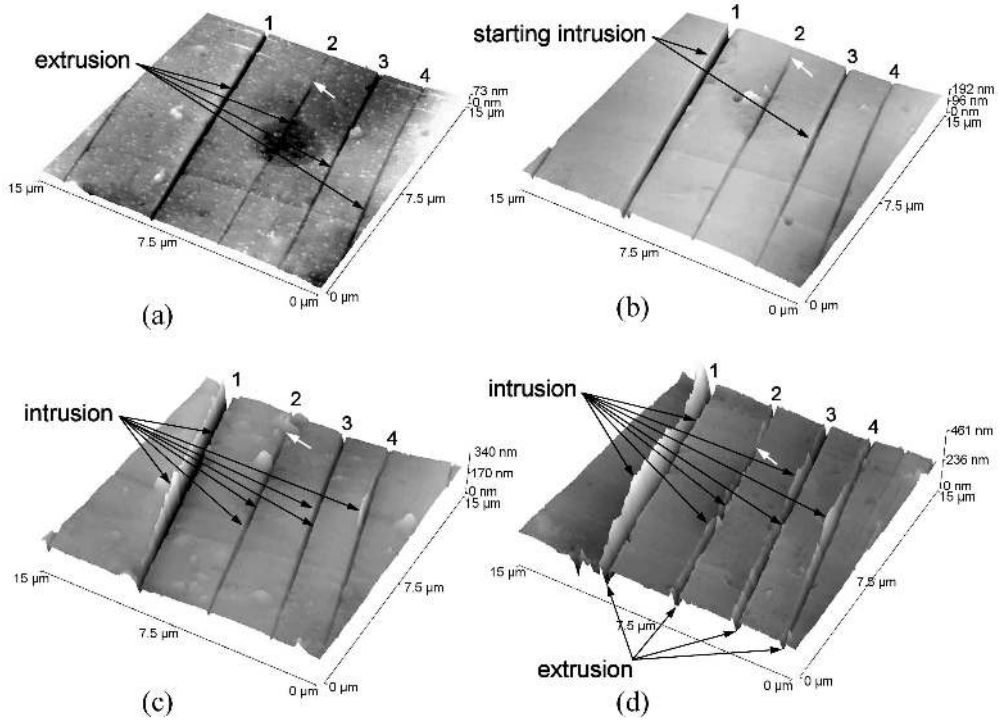

Figure 6. Early stages of surface relief evolution within the grain No. 78 of 316L steel cycled with $\varepsilon_{ap}=1x10^{-3}$ as obtained by AFM using plastic replicas. (a) N = 350 cycles (0.8% N_f), (b) N = 500 cycles (1.1% N_f), (c) N = 750 cycles (1.6% N_f), (d) N = 2000 cycles (4.3% N_f). The three-dimensional AFM micrographs of plastic replicas are displayed in non-inverted format.
107x77mm (600 x 600 DPI)

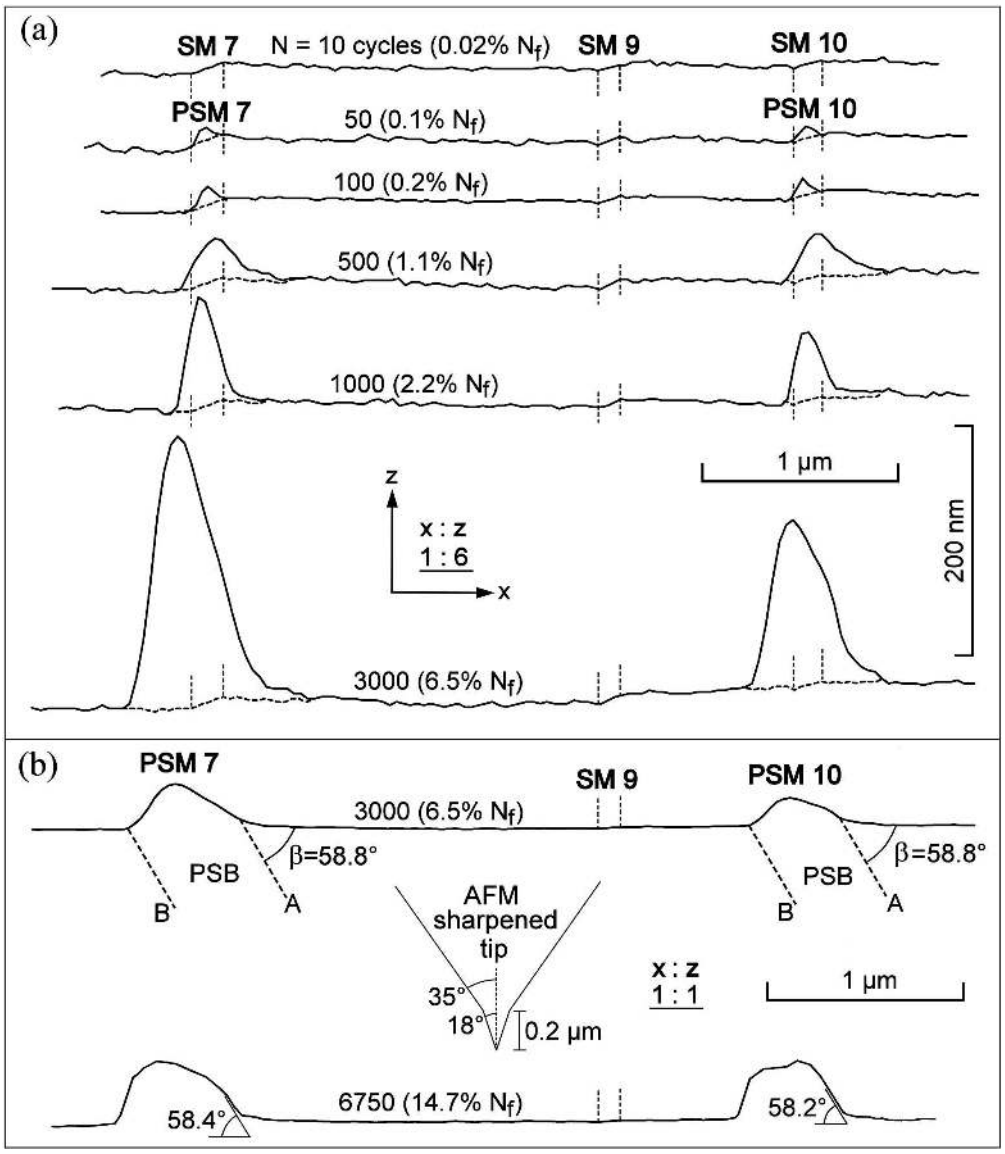

Figure 7. Development of surface relief profiles in the cross-section *A* marked in figure 5(e) as detected by AFM on the metallic specimen within the grain No. 62 of 316L steel cycled with $\varepsilon_{ap}=1x10^{-3}$. Profiles in the early and later stages are shown in the scale one-to-six (a) and one-to-one (b), respectively. The positions of fine SMs 7, 9 and 10 that appeared after 10 cycles are indicated by the vertical dashed lines; β is the angle of inclination of active slip plane to the specimen surface as calculated from EBSD measurements (see table 2).
146x167mm (600 x 600 DPI)

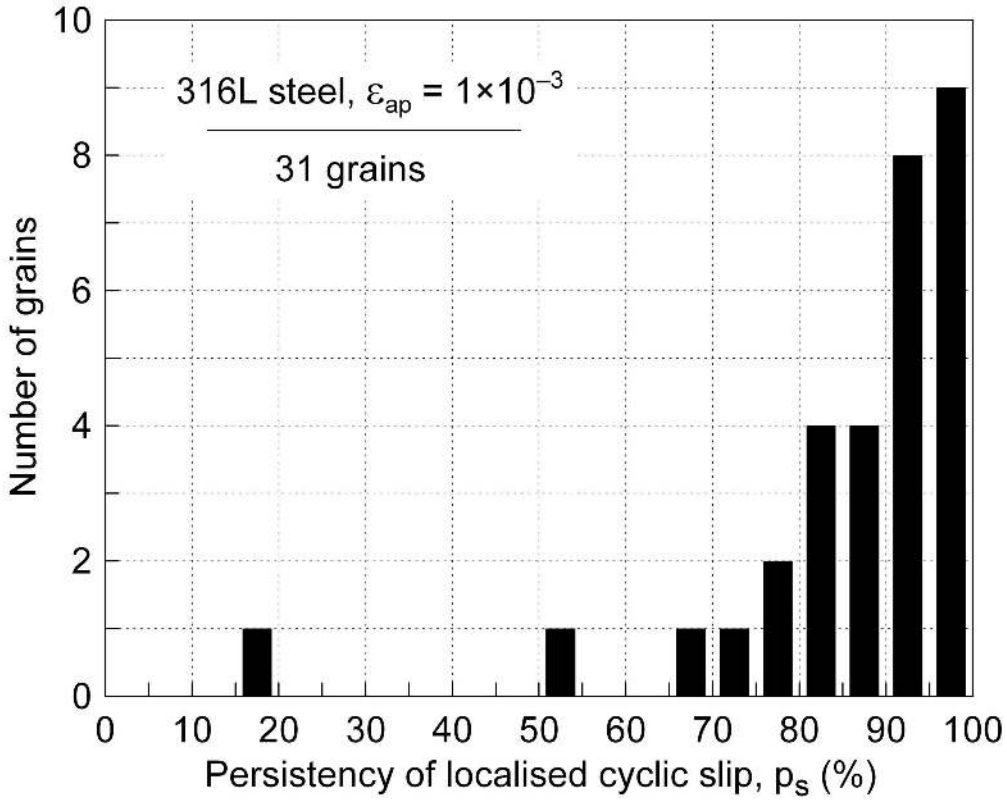

Figure 8. Number of grains with given persistency of localized cyclic slip, p_s, in specimen of 316L steel cycled with ε_{ap}=1x10^{-3}.
92x74mm (600 x 600 DPI)

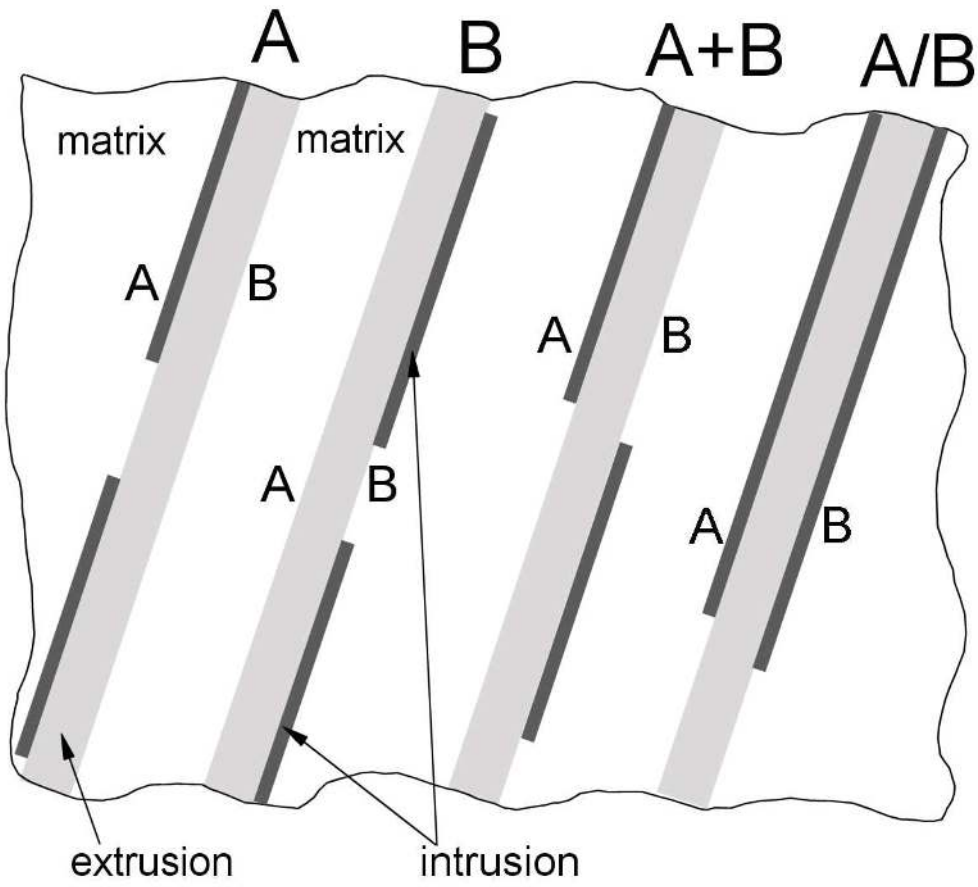

Figure 9. Typical configurations of extrusion-intrusion pairs observed in fatigued 316L.
75x67mm (400 x 400 DPI)

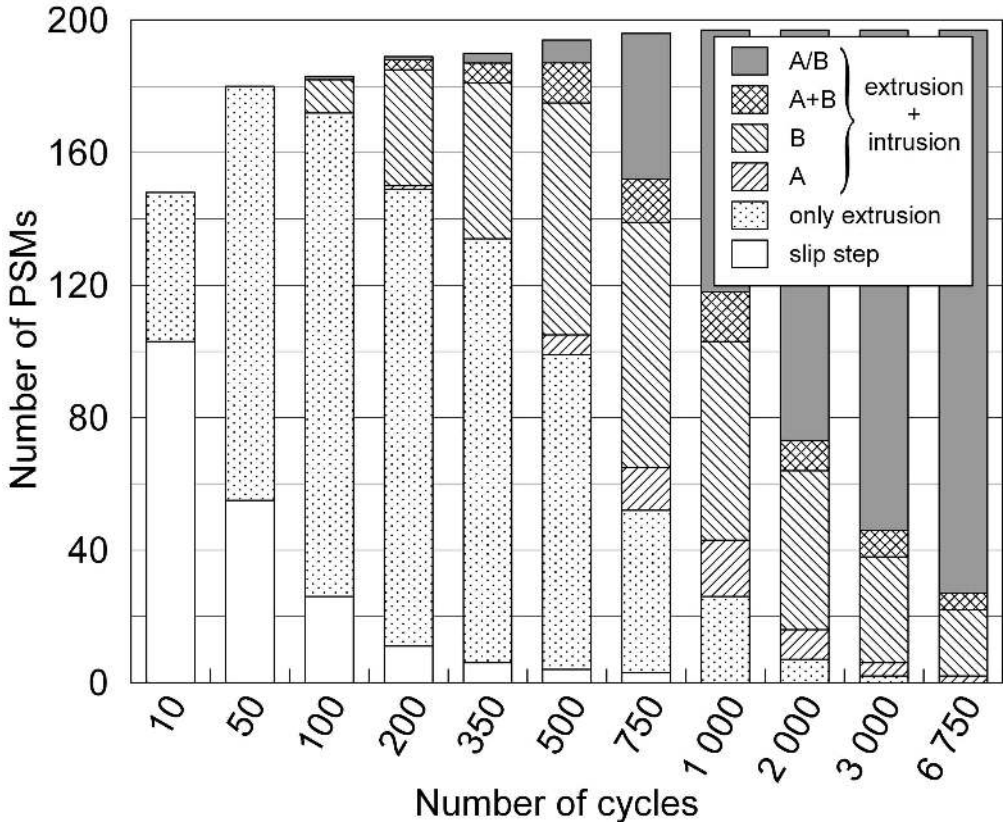

Figure 10. Evolution of morphology of 197 PSMs in 31 surface grains of 316L steel cycled with constant $\varepsilon_{ap}=1x10^{-3}$.
94x77mm (600 x 600 DPI)

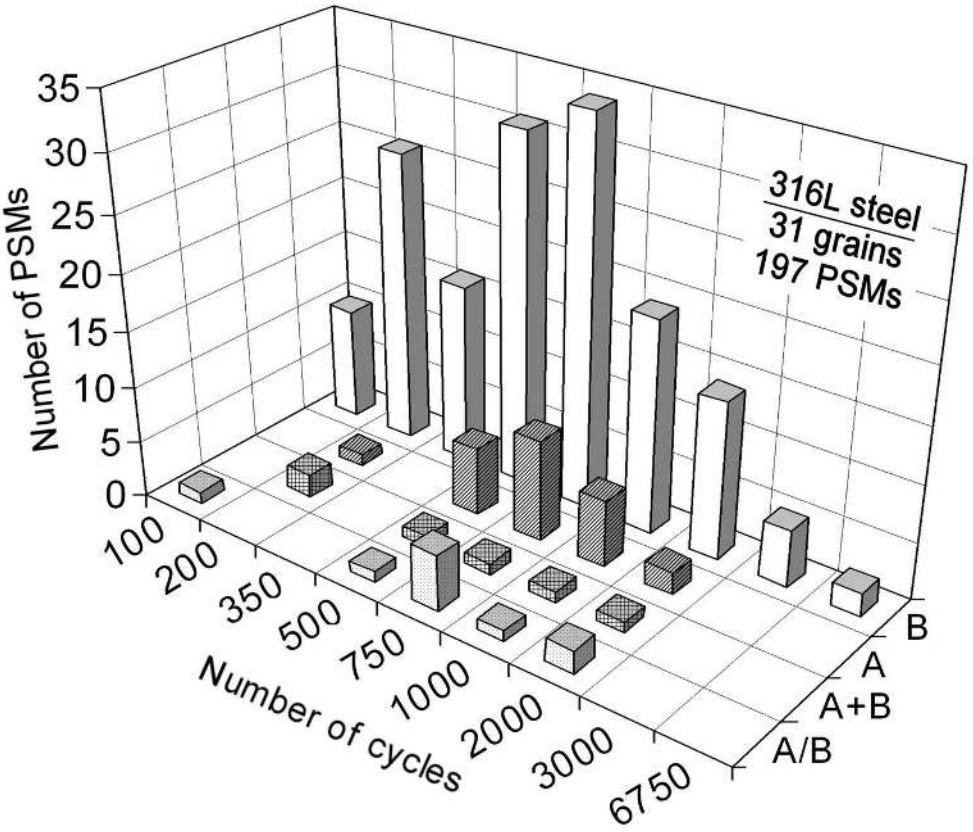

Figure 11. Occurrence of individual PSMs in 31 surface grains of 316L steel at the moment when the first intrusions appear.
59x50mm (600 x 600 DPI)

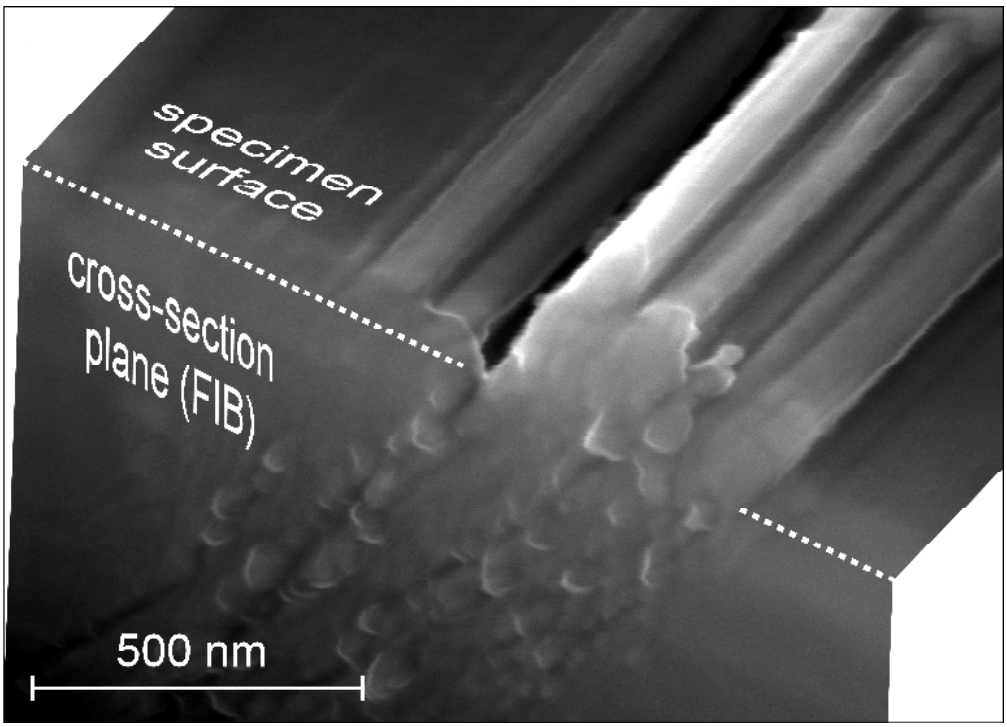

Figure 12. SEM-FEG micrograph of a cross-sectioned individual PSM in 316L cycled with $\varepsilon_{ap}=1x10^{-3}$. PSM was sectioned by FIB after 500 cycles and then fatigued to 2000 cycles.

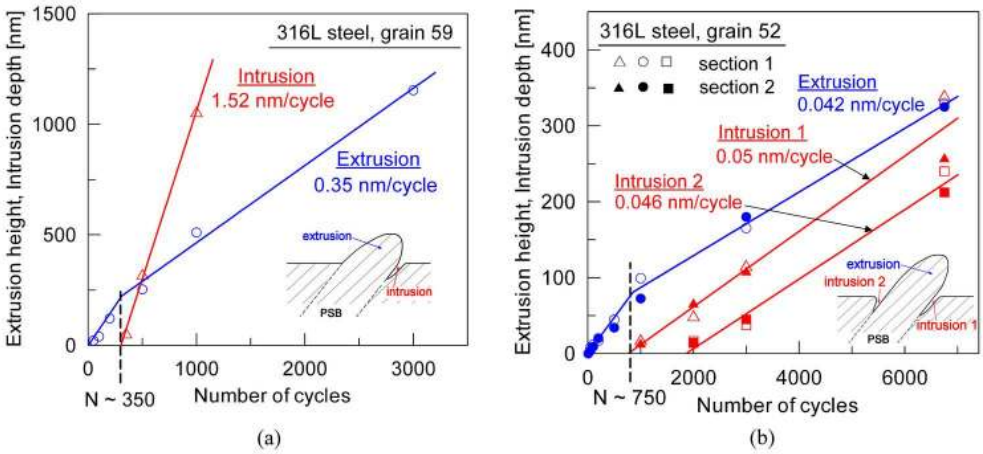

Figure 13. Simultaneous growth of extrusions and intrusions in the grains of 316L steel at the beginning of cycling with $\varepsilon_{ap}=1x10^{-3}$. (a) the grain No. 59 - extrusion and one parallel intrusion, (b) the grain No. 52 - extrusion and two parallel intrusions.
63x29mm (600 x 600 DPI)

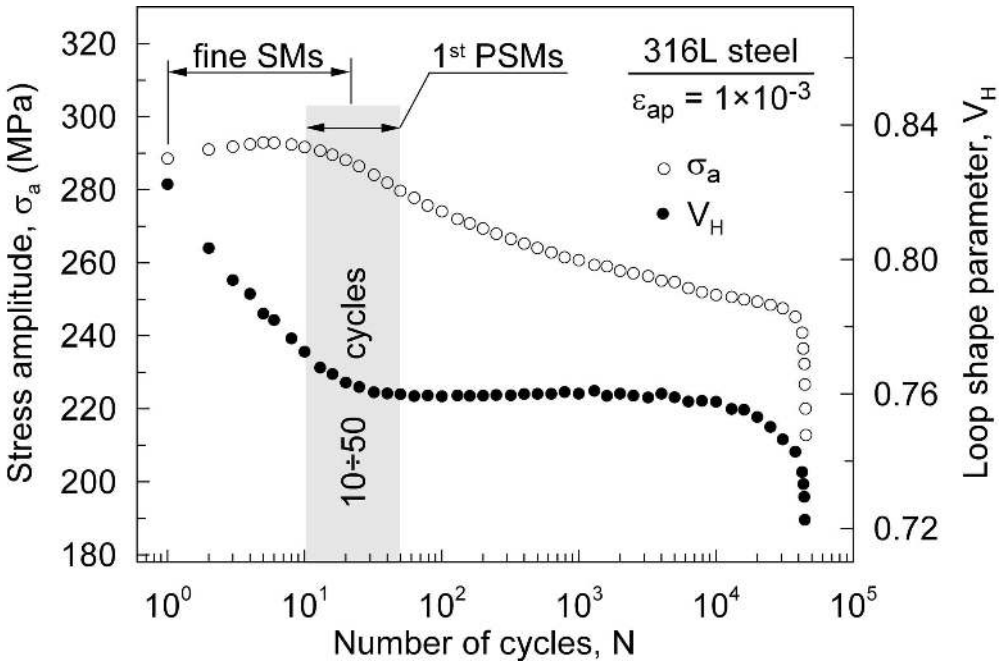

Figure 14. Correlation between the onset of PSM appearance, cyclic hardening/softening curve and the hysteresis loop changes characterized by the loop shape parameter V_H in 316L steel fatigued with constant plastic strain amplitude. SM - slip marking, PSM - persistent slip marking.
82x54mm (600 x 600 DPI)

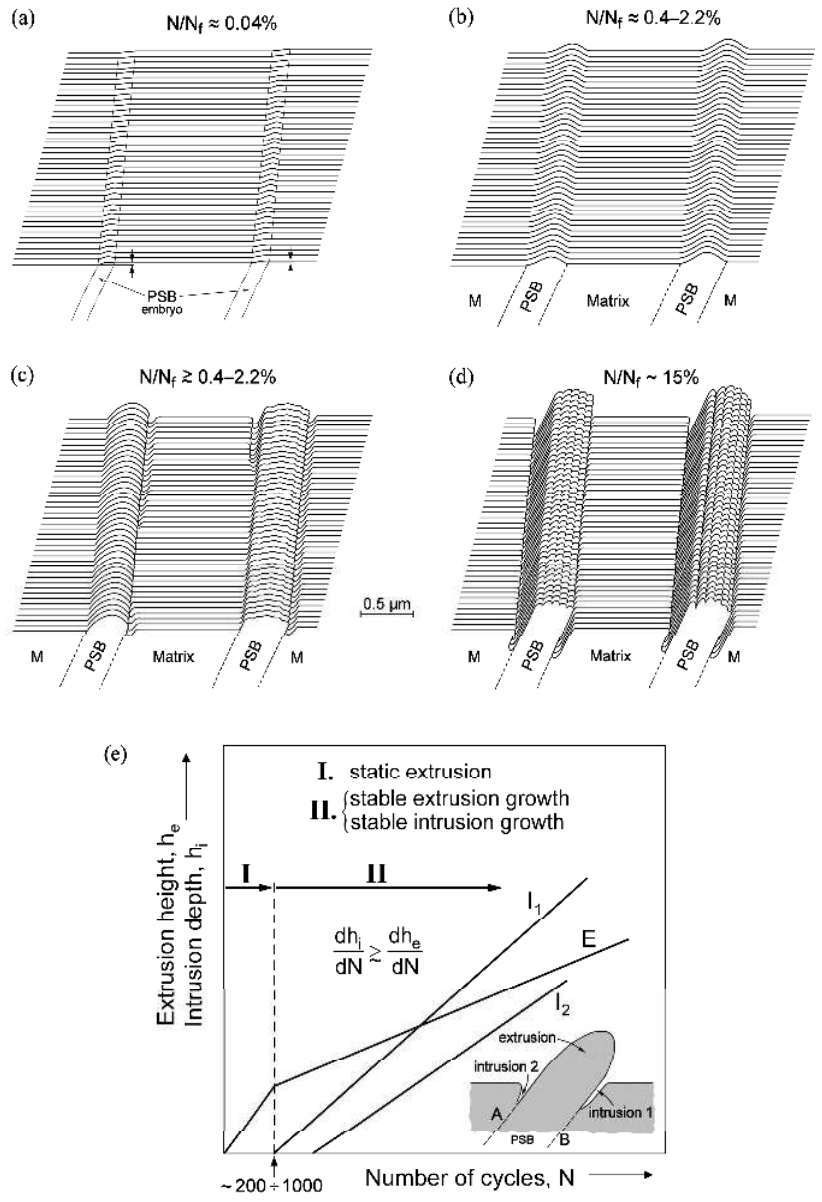

Figure 15. Schematic illustration of the consecutive characteristic stages of surface relief evolution in 316L steel fatigued with constant plastic strain amplitude of $1x10^{-3}$ at room temperature. (a) Fine SMs with tensile (and/or compressive) slip steps, (b) true PSMs with ribbon-like "static" extrusions, (c) growing extrusions and intrusions starting at PSB/matrix interfaces, (d) mature PSMs with well developed ribbon-like extrusions accompanied by two parallel intrusions at both PSB/matrix interfaces, (e) the kinetics of the growth of extrusions and intrusions.
143x210mm (600 x 600 DPI)